RECONSTRUCTION OF ATMOSPHERIC FLOWS BASED ON PROPER ORTHOGONAL DECOMPOSITION METHOD

A THESIS SUBMITTED TO
THE GRADUATE SCHOOL OF NATURAL AND APPLIED SCIENCES
OF
MIDDLE EAST TECHNICAL UNIVERSITY

BY

TANSU SEVINE

IN PARTIAL FULFILLMENT OF THE REQUIREMENTS
FOR
THE DEGREE OF MASTER OF SCIENCE
IN
AEROSPACE ENGINEERING

JANUARY 2017

Approval of the thesis:

RECONSTRUCTION OF ATMOSPHERIC FLOWS BASED ON PROPER ORTHOGONAL DECOMPOSITION METHOD

submitted by **TANSU SEVINE** in partial fulfillment of the requirements for the degree of **Master of Science in Aerospace Engineering Department, Middle East Technical University** by,

Prof. Dr. Gülbin Dural Ünver
Dean, Graduate School of **Natural and Applied Sciences** ________________

Prof. Dr. Ozan Tekinalp
Head of Department, **Aerospace Engineering** ________________

Prof. Dr. İsmail H. Tuncer
Supervisor, **Aerospace Engineering Department, METU** ________________

Assist. Prof. Dr. Mustafa Kaya
Co-supervisor, **Aerospace Engineering Dept., YBU** ________________

Examining Committee Members:

Prof. Dr. Yusuf Özyörük
Aerospace Engineering Department, METU ________________

Prof. Dr. İsmail H. Tuncer
Aerospace Engineering Department, METU ________________

Assoc. Prof. Dr. Sinan Eyi
Aerospace Engineering Department, METU ________________

Assist. Prof. Dr. Mustafa Kaya
Aerospace Engineering Department, YBU ________________

Assist. Prof. Dr. Gökhan Ahmet
Aerospace Engineering Department, OMU ________________

Date: ________________

I hereby declare that all information in this document has been obtained and presented in accordance with academic rules and ethical conduct. I also declare that, as required by these rules and conduct, I have fully cited and referenced all material and results that are not original to this work.

Name, Last Name: TANSU SEVINE

Signature :

ABSTRACT

RECONSTRUCTION OF ATMOSPHERIC FLOWS BASED ON PROPER ORTHOGONAL DECOMPOSITION METHOD

Sevine, Tansu
M.S., Department of Aerospace Engineering
Supervisor : Prof. Dr. İsmail H. Tuncer
Co-Supervisor : Assist. Prof. Dr. Mustafa Kaya

January 2017, 57 pages

The placement of wind turbines in a wind farm, which is called micro-siting, is a crucial task in regard to the maximization of the energy production in a wind farm. The maximum energy production is only possible if all the wind turbines are placed in optimum locations. Although the micro-siting of wind turbines has many aspects to be considered such as wind field analysis, wake effect of the other turbines and accessibility, the wind speed is the most significant parameter. The statistical wind speed distribution over a wind farm is currently reconstructed from a wind field analysis, which is mostly based on statistical analysis of wind field data collected from a meteorological mast and numerical simulations of wind fields over the wind farm. The reconstruction of wind fields is mostly based on an interpolation process.

In this study, a novel method based on the Proper Orthogonal Decomposition (POD) of fictitious wind fields is developed for the reconstruction of actual wind fields based on observation data. The fictitious wind fields for different wind sectors (wind direction) are obtained using an open-source Navier-Stokes solver, SU^2, on high resolution terrain fitted computational grids. The POD based reconstruction of flow fields is first validated in 2D flow fields. It is then implemented for the reconstruction of wind fields over a wind farm. It is shown that the methodology developed is capable of reconstructing wind fields over wind farms and can effectively be employed for micro-siting of wind turbines.

Keywords: Wind Energy, Computational Fluid Dynamics (CFD) , Proper Orthogonal Decomposition (POD), Open-Source Navier-Stokes Flow Solver (SU^2)

ÖZ

ATMOSFERİK AKIŞ ALANLARININ UYUMLU DİK AYRIŞIM YÖNTEMİYLE YENİDEN OLUŞTURULMASI

Sevine, Tansu
Yüksek Lisans, Havacılık ve Uzay Mühendisliği Bölümü
Tez Yöneticisi : Prof. Dr. İsmail H. Tuncer
Ortak Tez Yöneticisi : Yrd. Doç. Dr. Mustafa Kaya

Ocak 2017 , 57 sayfa

Rüzgar türbinlerinin rüzgar tarlalarınına yerleştirilmesi, yani mikro-konuşlandırma, rüzgar tarlalarından elde edilen enerjinin en üst seviyede olması için çok önemlidir. Maksimum enerji üretimi yalnızca rüzgar türbinlerinin, rüzgar tarlalarınındaki en verimli yerlere konuşlandırılmasıyla elde edilebilir. Rüzgar türbinlerinin mikro-konuşlandırması rüzgar alanı analizi, diğer türbinlerin girdap etkisi, ulaşılabilirlik vb. birden çok alanla ilgilenirken, rüzgar hızı tahmini bunların en başında gelir. Günümüzde rüzgar tarlalarının istatistiksel rüzgar hızı dağılımları, rüzgar alanı analizleri ile yeniden oluşturularak yapılmaktadır. Bu analizler, meteorolojik gözlem istasyonlarından elde edilen rüzgar alan verisinin istatistiksel olarak toplanmasıyla ve rüzgar tarlası üzerindeki rüzgar alanının nümerik yöntemlerle çözülmesi ile elde edilir. Rüzgar alanının yeniden oluşturulması ise genellikle aradeğerleme (interpolasyon) ile yapılır.

Bu çalışmada, rüzgar alanlarının yeniden oluşturulması amacıyla Uyumlu Dik Ayrışım (UDA) yöntemini kullanarak, simgesel nümerik çözümlere ve ölçüm verisine dayanan yeni bir yöntem geliştirilmiştir. Simgesel nümerik çözümler açık kaynaklı akış çözücü SU^2 ile yüksek çözünürlüklü topoğrafya üzerinde oluşturulmuş çözüm ağından giriş rüzgarının yönünün değiştirilmesiyle elde edilmiştir. Rüzgar alanlarının UDA yöntemine dayalı olarak yeniden oluşturulması öncelikle 2 boyutlu akışlar üzerinde doğrulanmıştır. Daha sonra rüzgar tarlaları üzerindeki atmosferik akış alanlarına

uygulanmıştır. Geliştirilen yöntemin atmosferik akış alanlarının yeniden oluşturmada kullanılabileceği ve rüzgar türbinlerinin mikro-konuşlandırma işleminde etkili bir biçimde çalıştırılabileceği gösterilmiştir.

Anahtar Kelimeler: Rüzgar Enerjisi, Hesaplamalı Akışkanlar Dinamiği (HAD), Uyumlu Dik Ayrışım Yöntemi (UDA), Açık-Kaynaklı Navier-Stokes Akış Çözücüsü (SU^2)

Yesterday is history.
Tomorrow is mystery.
Today is a gift.

ACKNOWLEDGMENTS

I would first like to thank my supervisor İsmail Hakkı Tuncer for his guidance and patience throughout the study.

I similarly would like to thank my co-supervisor Mustafa Kaya for his valuable contributions throughout the study.

I wish to express my sincere thanks to Gökhan Ahmet for his support and guidance throughout the study.

It would be impossible to complete this study without the support of my team mate and more importantly my big brother Engin Leblebici.

I would like to thank my lovely wife Cansu Sevine for her endless support and love in this period of my life.

I wish to express my sincere thanks to my mother and my sister for their thrust and understanding.

Finally, I dedicate this study to my respected father Ferat Sevine. I wish you could see these days, RIP my beloved dad.

TABLE OF CONTENTS

ABSTRACT v

ÖZ vii

ACKNOWLEDGMENTS x

TABLE OF CONTENTS xi

LIST OF TABLES xiii

LIST OF FIGURES xiv

LIST OF ABBREVIATIONS xvi

CHAPTERS

1 INTRODUCTION 1

1.1 Wind Farm Siting 2

1.1.1 Macro-siting of the Wind Farms 2

1.1.2 Micro-siting of the Wind Farms 2

1.1.3 Micro-siting with WindSim 4

1.2 Proper Orthogonal Decomposition Method 6

1.3 Objectives of The Study 7

2 METHODOLOGY 9

2.1 Proper Orthogonal Decomposition of Flow Fields 10

2.1.1 Low Memory Singular Value Decomposition . . . 12

2.2 SU^2 (Stanford-University-Unstructured) - Open Source Flow Solver 14

2.2.1 Governing Equations 14

2.3 Discretization of Computational Domain 16

2.3.1 Smoothing and Extension of Terrain 17

3 RESULTS AND DISCUSSION 19

3.1 Reconstruction of 2D Flow Fields 19

3.1.1 Reconstruction of Airfoil Surface Pressure Distribution 21

3.1.2 Reconstruction of Airfoil Surface Pressure Distribution at an Arbitrary Angle of Attack 22

3.1.3 Reconstruction of 2D Pressure Fields 25

3.2 Reconstruction of Atmospheric Flow Fields 27

3.2.1 Flow Fields Computed by SU^2 27

3.2.1.1 Grid Generation 28

3.2.1.2 Flow Models and Boundary Conditions 28

3.2.1.3 Parallel Performance 34

3.2.2 POD Based Reconstruction of Flow Fields 35

3.3 Comparison with WindSim Predictions 40

4 CONCLUSIONS 53

LIST OF TABLES

TABLES

Table 3.1 SU^2 Parallel Performance 35

Table 3.2 Z axis cuts and corresponding vertical distances 36

Table 3.3 Dominance of the POD modes as a function of number of solutions in the dataq set 38

Table 3.4 Distribution of the first 10 nodes in z-direction 40

LIST OF FIGURES

FIGURES

Figure 1.1 WindSim solution strategies [27] 5

Figure 2.1 Flow field edge length contours in z-direction and its histogram . . 17

Figure 2.2 Smoothing and extension of the computational domain: Purple: Terrain surface over the wind farm, Green: Extended computational surface. 18

Figure 2.3 Extended computational domain – definition of inlet flow, approach flow and incident flow [4] 18

Figure 3.1 Computational grid and convergence of residuals with respect to angle of attack 20

Figure 3.2 Reconstruction of existing C_p distribution at $\alpha = 3°$, $M = 0.2$ . . 22

Figure 3.3 Interpolation of POD coefficients ω for an arbitrary angle of attack . 23

Figure 3.4 Reconstruction of C_p distribution for at $\alpha = 1.5°$, $M = 0.2$ 24

Figure 3.5 Reconstruction of C_p distribution for at $\alpha = 1.5°$, $M = 0.2$ with respect to data set size 24

Figure 3.6 Reconstruction of pressure field using increasing number of POD modes at $\alpha = 1.5°$, $M = 0.2$ 26

Figure 3.7 Interested solution region, the wall surface grid and elevation maps of central region and extended region of Mut region in Mersin/Turkey . . 29

Figure 3.8 Computational domain of Mut region in Mersin/Turkey 30

Figure 3.9 SU^2 solver options: a)-flux splitting algorithms and linear solvers, b)-boundary conditions, c)- configuration ".cfg" file 31

Figure 3.10 Inflow-uutflow and wall boundaries 32

Figure 3.11 WRF Solution for 1-day with $\delta t = 5min$ 33

Figure 3.12 SU2 and WRF wind speed comparisons 34

Figure 3.13 SU^2 parallel speed-up 35

Figure 3.14 Computational domain of size $244 \times 145 \times 30$ vs. Reduced domain of size $88 \times 187 \times 14$ used in reconstruction 36

Figure 3.15 Comparison of reconstructed velocity fields with SU^2 solution at 30m, 60m and 100. 39

Figure 3.16 Digital terrain model - elevation (m) and roughness height (m), WindSim 40

Figure 3.17 Digital terrain model - grid (z), WindSim 41

Figure 3.18 0° sector solution comparison of WindSim and SU^2 at 60m above ground level 42

Figure 3.19 90° sector solution comparison of WindSim and SU^2 at 60m above ground level 43

Figure 3.20 180° sector solution comparison of WindSim and SU^2 at 60m above ground level 44

Figure 3.21 270° sector solution comparison of WindSim and SU^2 at 60m above ground level 45

Figure 3.22 Wind speed variation above ground distribution of WindSim at 3 different locations and average wind speed of the all points on the wall surface 47

Figure 3.23 MET-MASTlocation in the domain, $x = 521404m, y = 4085462m$. 48

Figure 3.24 SU^2 vs. POD and WindSim wind speed vs. height distribution at the MET-MAST location, $x = 521404\ m, y = 4085462\ m$ 48

Figure 3.25 SU^2 vs. POD and WindSim wind speed contours [m/s]. 30 meters above from the ground level 49

Figure 3.26 SU^2 vs. POD and WindSim wind speed contours [m/s]. 60 meters above from the ground level 50

Figure 3.27 SU^2 vs. POD and WindSim wind speed contours [m/s]. 100 meters above from the ground level 51

Figure 3.28 SU^2 vs. POD and WindSim wind speed contours [m/s]. 150 meters above from the ground level 52

LIST OF ABBREVIATIONS

CFD	Computational Fluid Dynamics
POD	Proper Orthogonal Decomposition
SU2	Stanford University Unstructured
WRF	Weather Research Forecast
RANS	Reynolds-Averaged Navier-Stokes
AEP	Annual Energy Production
WAsP	Wind Atlas Analysis and Application Program
MOR	Model Order Reduction
PDE	Partial Differential Equation
PCA	Principal Component Analysis
SVD	Singular Value Decomposition
ϕ	POD Modes (Eigenvectors)
ω	POD Mode's Coefficients
$\tilde{\omega}$	POD Mode's Proper Coefficients
U	Vector of State Variable
$\vec{F}^c(U)$	Convective Flux Cector
$\vec{F}^v(U)$	Viscous Flux Vector
$Q(U)$	Source Term
ρ	Density
u	Velocity in x-direction
v	Velocity in y-direction
w	Velocity in z-direction
T	Temperature
P	Pressure
τ	Shear Stress
μ	Viscosity
H	Entalphy
C_p	Pressure Coefficient
α	Angle of Attack

CHAPTER 1

INTRODUCTION

The demand for the energy in industry and in urban life style is growing day by day. Such a demand increases the public awareness of environmental concerns about clean energy resources. Thus, conventional fossil fuels are being replaced by renewable energy supplies which are clean, and environmentally friendly [16, 23]. Among the renewable energy sources such as wind energy, solar energy, biomass, hydro power, geothermal, the wind energy is currently taking more attention than the others due to its low cost, sustainability and high availability.

Wind energy is obtained through a wind turbine. Industrial wind energy production is derived from a large number of turbines installed in a wind farm, where the wind resource is available and sustainable. Once the macro-siting of a wind farm is made, the placement of individual wind turbines in the farm, which is know as micro-siting, becomes the main challenge. The main objective of a macro and micro siting of a wind farm is to maximize the energy production while minimizing the unit cost of energy[12].

As the size of wind turbines grows for higher efficiency and reduced cost of energy, the cost of a single wind turbine installation grows as well. it is therefore quite important to place each wind turbine in a wind farm at an optimum place where the local wind speed is the highest, and the energy production of the turbine is maximum.

1.1 Wind Farm Siting

There are two important processes in the wind farm site selection, namely macro-siting and micro-siting of a wind farm. Macro siting is the process of determining the location of windy places based on wind atlases, which are mostly produced based on long term meteorological observation data and on meso-scale atmospheric flow simulations performed with global weather forecasting models such as WRF and MM5.

1.1.1 Macro-siting of the Wind Farms

Candidate sites for a wind farm are first selected on the basis of a wind atlas or of wind fields predicted by meso-scale weather prediction models. The sites selected are then validated with field measurements. The wind field data in terms of statistical wind speed and wind direction are used to estimate the energy production potential of the field. Such a determination of a wind farm site process is called macro-siting.

The macro-siting tools are very powerful for the site selection of wind farm , but they lack precision for the placing of wind turbines into the best position within the farm. In order to maximize the total power output from the wind farm, micro-siting of wind turbines is essential[26]. High resolution wind resource maps, which are needed for the micro-siting of wind turbines are currently obtained by means numerical flow simulations over the wind farm and the corrections based on long term wind field measurements.

1.1.2 Micro-siting of the Wind Farms

Meso-scale meteorology is generally deals with 5 km to 200 km spatial resolution in the atmosphere, while micro-scale meteorology is the study of less than 5 km [8]. Micro-siting deals with the specific properties of a wind turbine and the magnitude and direction of the wind speed, which is affected by any obstruction in the wind field and terrain features.

A well-known micro-scale flow simulator WAsP [10] is based on inviscid, linearized flow models. Such linearized tools are suitable for off-shore, flat wind fields, but they do not perform well on complex terrains, where the wind flow may separate on the terrain surface forming large scale vertical structures. Therefore, the wind fields on the complex terrains cannot be captured by linearized flow models. Use of such models on complex on-shore terrains may causes wind turbines to be installed in sub-optimal places, which results in reduced power output. It should be noted that the wind power is proportional with the cube of the wind speed. Even very small rise in the wind speed, increases the energy production significantly.

In general, high wind speeds occur at mountainous regions and ocean shores. Although meso-scaled traditional methods like wind atlases,and linearized micro-scale models are widely used in the wind industry, they cannot capture sudden changes of the terrain complexity and wind speed of that location. Most of the mountainous regions are complex terrains and they need to be analyzed with high resolution terrain data in order to capture the orographic winds efficiently. For an accurate simulation of wind fields over complex terrains non-linear flow models with high resolution elevation data become a requirement for the wind industry. High-resolution wind field data for the entire wind farm is needed for a successful micro-siting of wind turbines.

For a successful micro-siting a satisfactory high resolution flow-field analysis with current CFD tools and a proper topographical modeling are necessary [2]. Field measurements and accurate CFD simulations of wind fields may be used together for the reconstruction of atmospheric flow fields [6]. Local winds are often monitored for a year or more, and different sectors numerical solutions are performed for high resolution digital elevation model (DEM) data, in order to construct detailed wind resource maps of whole flow field.

There are numerous numerical models used in the wind energy industry, the most common ones can be specified as linearized models, Reynolds Averaged Navier Stokes (RANS) Models, Large Eddy Simulation (LES) models, Direct Numerical Simulation (DNS) models. LES and DNS based tools give better results but they are computationally expensive.

To construct flow fields over wind farms there are quite a few commercial or non-commercial software such as WAsP, WindSim, Openwind.

WAsP is a software built for wind power production estimation and wind climate prediction [1]. It is a linearized micro-scale flow model and makes simply vertical and horizontal extrapolation of statistical wind data. It has several models to describe the wind flow over different terrains and close to sheltering obstacles [19].

WAsP firstly analyses time-series of wind speed and direction obtained from pre-measured statistical raw wind data, and extracts the wind climate of the region. Secondly, using the regional wind climate and site description, it predicts the wind climate. Then using this information predicts the annual energy production (AEP) of wind turbine using its power curve.

WAsP and other linearized models are used widely in wind industry because they are powerful tools for the solution of atmospheric flow field of non-complex regions. However, in the mountainous regions these linearized tools are not enough to capture the complex wind fields. For complex terrains and flow fields CFD based tools are required. Solving Navier-Stokes equations in a high resolution computational domain provides accurate wind fields.

CFD is not the only way of obtaining wind fields in a wind farm. An average wind field may also be constructed based of the measurement of wind speed and direction at certain points, and fictitious flow field obtained with CFD tools. Popular commercial software in wind industry such as WindSim, Meteodyne, WAsP-CFD, employ such an approach to reconstruct wind fields in wind farms.

1.1.3 Micro-siting with WindSim

WindSim is a CFD based commercial software using for local atmospheric flow field predictions. Solving 3D Reynolds Averaged Navier-Stokes equations makes WindSim a suitable tool for simulations in complex terrain, and in situations with complex local climatology [9]. For the WindSim solution process, firstly terrain model is generated based on digital elevation models, roughness maps and user inputs such as height above terrain, height distribution factor number of cells in the z-direction and so on. Secondly, the simulation of the wind fields are obtained using the terrain model created. The wind fields are constructed by solving the RANS equations. The

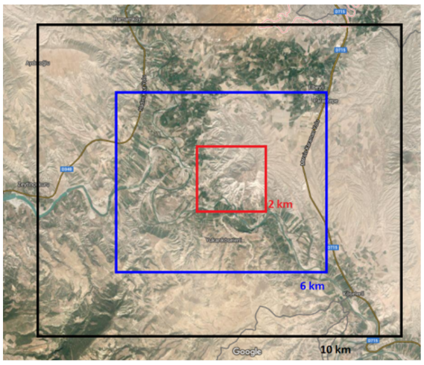

(a) Nesting

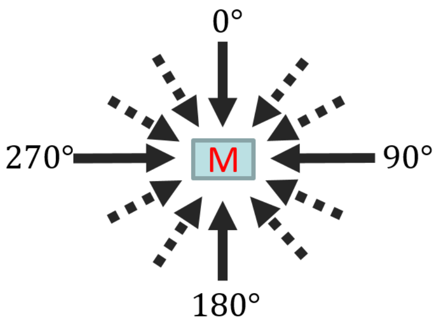

(b) Sectoring

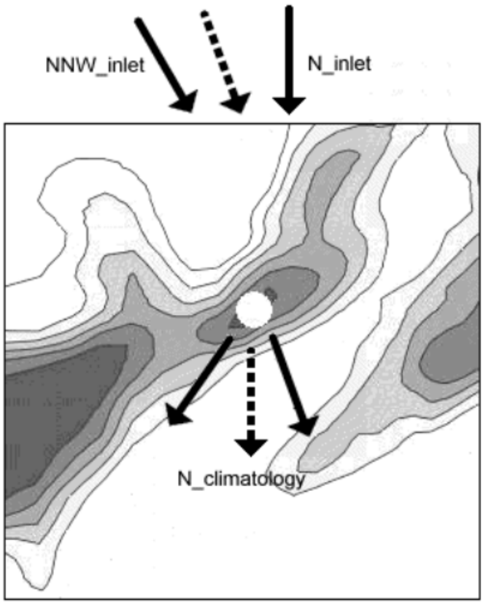

(c) Sector Interpolation

Figure 1.1: WindSim solution strategies [27]

k-epsilon is applied as turbulence model. Since the RANS equations are non-linear, iterative solution procedure is applied, and steady wind fields are obtained for a given number of sectors. Every sector solutions are obtained from different CFD cases with different wind direction, hence sectoring process is a computationally costly depending on the mesh resolution [2]. Because running simulations at least 12 different input with a big grid takes quite much time.

WindSim uses the fictitious flow fields and the time series of observation data as a climatology correction for obtaining the wind resource maps. The wind resource map is established by weighting the wind database against the climatology by an inverse distance interpolation process (Figure 1.1) [17, 27].

1.2 Proper Orthogonal Decomposition Method

Proper Orthogonal Decomposition (POD) is a powerful and elegant method for data analysis which aims to extract dominant characteristics of the high-dimensional dataset [15]. POD method is a recent study field and applications of POD for different areas are exist. For example, POD has been used in various disciplines in terms of image processing, signal analysis, data compression, process identification and control in chemical engineering, oceanography, etc. [11]. In addition to these applications, POD is used to analyze experimental data with the objective of extracting dominant features [5].

Schilders mentioned that POD is a kind of Model Order Reduction (MOR), POD is also known as Karhunen-Loeve decomposition, Principal Component Analysis (PCA), and singular value decomposition (SVD) [24]. According to Liangs' [15] and Ahmet's study [3] , the original data can be approximated or reconstructed by using less number of dominant modes (i.e. eigenvectors). This technique is also known as Model Order Reduction, and used for various cases such as data compression (ZIP,RAR), communication, sending information from space and so on. For communication people generally use cell phones or PCs to talk with each other. Cell phones and computers have microphones to hear speeches. They convert pressure variations (sounds) into the electrical signals corresponding to pressure intensity. Computers process those signals around 40000 times per second by measuring the amplitude of the signals. The storage of the measurements require serious memory because each of them are stored as 16 bit in general. Sending those data to the person other side of the computer or phone requires too much time. So instead of sending the whole data, sending only the reduced eigenvalues of them is making the process so quicker as long as the eigenvectors of the voice data is embedded on the computers or the cell phones. As the number of dominant modes increased in the sent data, the voice reach more clear to the other side. This is the reason why walkie-talkie voice is dirty and current cell phones' voice is clear. For the transmitting voice, walkie-talkies use less number of dominant modes than cell phones which leads the cell phones have clear voice. Sirovic discovered the method of snapshots which is used on face recognition. The method simply calculates the dominant characteristics of the face pictures in the database, then based on those dominant characteristics he can obtain whole face pictures with only providing face parts. Main point of POD in his study is, instead of calculating dominant characteristics of all face pictures in the database which is beyond the limits of the current computers $(2^{14} \times 2^{14})$, he uses very small number $(M \times M, M = 115)$ for the reconstruction of the face pictures resulting less 10 percent error . The details of his study can be found from [25].

POD method is developed within the area of Computational Fluid Dynamics and nowadays used frequently in many problems [24]. As it well known CFD is computationally costly process in terms of memory and computation time. Therefore method of snapshots, introduced by Sirovic, is started to use in CFD calculations especially for aerodynamic calculations [20, 21]. In this thesis Sirovic's method of snapshots technique is applied for the reconstruction of atmospheric flow field . He used different numerous image portraits, but we use different sector solutions as snapshots. Just like Sirovic calculated the dominant characteristics of the face pictures in the database, we are going to calculate dominant flow characteristics in the database obtained by the snapshots. Then based on them, the atmospheric flow field will be reconstructed with providing flow solutions only some part of the computational domain.

1.3 Objectives of The Study

The thesis work aims at developing a POD based tool for the reconstruction of the atmospheric flow field and the generation of wind resource maps to be used in micrositing of wind turbines. Similar to the commercial tools available, the present method will extract dominant flow characteristics from the wind fields simulations along the different sectors of the wind farm. The open source Navier-Stokes solver SU^2 will be eployed for the simulation of wind fields. Many of the commercial wind assessment tools use sectoring strategy, then for the correlation part they generally use interpolation corrected with the field measurement data. In this study, instead of interpolation, a POD based method wil be developed for the reconstruction of the wind fields.

In the content of this thesis, firstly, the methodology of the study is introduced, namely the POD method, SU^2 open-source flow solver and discretization of the computational domain over wind farms. Next, as a preliminary and validation study, POD technique is applied to the reconstruction of 2D flow fields. 3D atmospheric flow fields are then obtained with the SU^2 solver along different sectors of the wind farm and the POD method is applied to these sector solutions for the reconstruction of the wind field based on wind data at a single or several observation points. The reconstructed wind fields are compared againsts the WindSim predictions.

CHAPTER 2

METHODOLOGY

In this study atmospheric flow solutions based on a Navier-Stokes solver are used together with the Proper Orthogonal Decomposition (POD) method for the reconstruction of the wind fields over wind farms.

The wind fields over wind farms, which are needed for micro-siting of wind turbines, are reconstructed based on the statistical wind data obtained from a met-mast installed within the wind farm. The main challenge is to reconstruct the average wind field over the wind farm based on the wind speed and direction given at certain locations.

This is currently achieved by correlating fictitious sectoral flow solutions, which are obtained with CFD tools and cover all the possible flow directions, with the measured data. CFD based wind fields are first corrected with regional wind climate data such as shelter from nearby obstacles, effect of roughness, effect of buoyancy [13]. The corrected flow solutions are then weighted with the statistical wind data for the reconstruction of the dominant wind field over the wind farm. The weighting process is nothing but an interpolation of the sectoral flow solutions according to the dominant wind characteristic of the region obtained by field measurements.

In this study, the weighting or interpolation process is replaced with the POD based reconstruction. The sectoral flow solutions are obtained by the open source Navier-Stokes flow solver SU^2. This chapter includes the main specifications and explanations of the tools necessary for solution and reconstruction of atmospheric flow fields . They can be listed as follows:

- Proper Orthogonal Decomposition (POD) Method

- SU^2 (Stanford-University-Unstructured) - open source flow solver
- Discretization of the computational domain

2.1 Proper Orthogonal Decomposition of Flow Fields

The POD method is currently used for various applications, such as inverse design problems, face recognition, communication,data compression, derivation of reduced order models and so on. POD method is not only used for the reconstruction of current data but also used for approximating the missing data. Reconstruction of current (i.e. existing) data is nothing but the Model Order Reduction technique. Same data is reconstructed by using reduced models. On the other hand, missing data case is reconstruction of unknown data using the known values. For big problems obtaining the whole data is generally difficult due to lack of information. For example, the method of snapshots technique[25], introduced by Sirovic, can be used for the determination of the dominant POD modes for big problems which requires large memory and computational cost. Sirovic obtains the face portraits by providing only some part of the faces based on snapshot technique. To reduce the cost and obtain the unknown flow properties is started to be used in CFD especially for aerodynamic calculations [20, 21].

In this thesis Sirovic's method of snapshots technique is applied for the reconstruction of atmospheric flow field . In his study the data set is created from lots of image portraits, whereas in this study data set is created from sector solutions of the atmospheric flow field. Sirovic calculated the dominant characteristics of the face pictures in the data set, similarly, the dominant flow characteristics of the sector solutions are calculated by POD method. Those dominant characteristics are nothing but the eigenvectors of the data set , and they are called POD modes. Then based on dominant modes, the atmospheric flow field will be reconstructed with providing flow solutions only some part of the computational domain. As POD method requires snapshots, in other words state solutions, the atmospheric flow field is obtained for 12 different sectors to construct the data set. Simulations carried out by SU^2 flow solver for an interested region where wind farm is planned to set up. Once dominant POD modes are calculated from snapshots, the original data or missing data can be reconstructed using these modes [3]

Let's say $[X]$ represents data set of the atmospheric flow field solutions with n sector and the computational domain has m number of nodes. The data set $[X]$ can be expressed in Equation 2.1 (Singular Value Decomposition) in terms of orthogonal vectors and singular values.

$$[X]_{m\times n} = [U]_{m\times m}[S]_{m\times n}[V]^T_{n\times n} \tag{2.1}$$

In the SVD calculation in Equation 2.1, $[S]$ is the singular values, in other words the square root of eigenvalues of the correlation matrix of X, $[C] = [X][X]^T or [C] = [X]^T[X]$. $[U]$ corresponds to left orthogonal vectors and $[V]$ corresponds to right orthogonal vectors of $[X]$. The multiplication of singular values and right orthogonal vectors are called as coefficient of the POD modes or pod coefficients, and they are represented with ω_i (Equation 2.2).

$$[\omega]_{m\times n} = [S]_{m\times n}[V]^T_{n\times n} \tag{2.2}$$

Then each columns of the data set matrix is defined as follows:

$$\vec{X_i} = [\omega_{1,i}\vec{U_1} + \omega_{2,i}\vec{U_2} + \cdots + +\omega_{m,i}\vec{U_m}]\ ; \quad i = 1, 2, ..., n \tag{2.3}$$

According to Liangs' and Ahmet's study, the original data $[X]$ can be approximated or reconstructed using k number of POD modes in other words orthogonal vectors, where k is very smaller than m. Let's define a reconstruction or approximation vector $\tilde{\vec{X}}$ which is the same data vector in the data set, to be reconstructed. Reconstruction vector $\tilde{\vec{X}}$ can be expressed by dominant k number of reduced orthogonal modes, $[U_{red}] = [\vec{U_1} \ \ \vec{U_2} \ \ \cdots \ \ \vec{U_k}]$,and k number of reduced proper coefficients ω as follows [15, 3]:

$$\tilde{\vec{X}} = [\omega_1\vec{U_1} + \omega_2\vec{U_2} + \cdots + \omega_k\vec{U_k}], \quad k << m \tag{2.4}$$

If reconstruction of the whole data can be obtained with only providing some part of the data, problem like face recognition from face parts, reconstruction of atmospheric flow field can be obtained from providing solutions at several points in the computational domain. Equation 2.4 defines the reconstruction vector of existing data, but for the reconstruction of missing data case the Equation 2.4 needed to be rewritten as Equation 2.5.

$$\tilde{\tilde{X}} = [\tilde{\omega}_1\vec{U}_1 + \tilde{\omega}_2\vec{U}_2 + \cdots + \tilde{\omega}_k\vec{U}_k], \quad k << m \tag{2.5}$$

Essential part of the reconstruction of the missing data case is, the determination of proper coefficients ($\tilde{\omega_i}$) of POD modes for reconstruction. $\tilde{\omega_i}$ values can be obtained from solving the least square equation (Equation 2.2). The procedure of the POD technique starts with finding dominant POD modes $\vec{U}_i$ and corresponding proper coefficients, $\tilde{\omega_i}$, where $i = 1, 2, ..., k$. Obtaining best approximation while keeping k minimum is the main purpose of the method. While POD modes give the direction of spread of data, singular values are the intensity of spread in a particular direction or in other words of that respective orthogonal vector. Descending sort of the related singular values shows the intensity of the singular values. Based on this, dominance of the k singular values over m singular values are calculated (Equation 2.6). This dominance r_k value is also valid for orthogonal vectors because orthogonal vectors and singular values are related with each other. Higher dominance value means increase in the approximation accuracy, hence, decreasing in the error.

$$r_k = \frac{norm(s_{1,m})}{norm(s_{1,n})} \tag{2.6}$$

Another important process in the POD reconstruction is determination of the k value. As the number of dominant POD modes k used for reconstruction increases the accuracy; but, it also increases the computation time and memory usage. Therefore, in order to find the best value for k, it has to be decided that how much error can be tolerated. Once the error is decided, automatically the desired accuracy of the approximation and then dominance value r_k is obtained. Then by solving Equation 2.6 for $r_k \geq 0.95$ (5%), best value of k can be found for desired tolerance.

2.1.1 Low Memory Singular Value Decomposition

For large data sets which require large computer memory to store the dominant modes can be evaluated from a correlation matrix instead of the original data set. The correlation matrix $[C]$ is nothing but the multiplication of the data set with its transpose or vice versa (Equation 2.7).

$$[C] = [X][X]^T \quad or \quad [C] = [X]^T[X] \tag{2.7}$$

The square root of the singular values and the corresponding orthogonal vectors of the correlation matrix are the same with the singular values and the orthogonal values. For the case $m > n$ the correlation matrix is taken in the following form:

$$[C]_{n\times n} = [X]^T_{n\times m}[X]_{m\times n} \tag{2.8}$$

Substituting $[X] = [U][S][V]^T$ into the above equation provides,

$$[C]_{n\times n} = \left([V][S]^T[U]^T\right)\ \left([U][S][V]^T\right)$$

$$[C]_{n\times n} = [V][S]^T[S][V]^T$$

$$[C]_{n\times n} = [V][S^2][V]^T \tag{2.9}$$

Also, obtaining the SVD of correlation matrix $[C]$,

$$[C]_{n\times n} = [\bar{U}][\bar{S}][\bar{V}]^T \tag{2.10}$$

Then equate Equation 2.9 and Equation 2.10 each other,

$$[C]_{n\times n} = [V][S^2][V]^T = [\bar{U}][\bar{S}][\bar{V}]^T$$

$$[V] = [\bar{U}];\ [S^2] = [\bar{S}];\ [V]^T = [\bar{V}]^T \tag{2.11}$$

Equation 2.11 shows that correlation matrix $[C]$ and data set $[X]$ have same right orthogonal vectors, which means that reconstruction can be done by using the SVD of correlation matrix instead of SVD of the whole data set. Then reconstruction part will be carried out by multiplication of the right orthogonal vectors with matrix $[X]$ and proper coefficient $\tilde{\omega_i}$ (Equation 2.12). In the low memory SVD process, because of right orthogonal vectors are used, the reconstruction is done by multiplication of proper POD coefficients by $[V]$ and matrix $[X]$.

$$\tilde{\tilde{X}} = [X]\vec{V}_1\tilde{\omega}_1 + [X]\vec{V}_2\tilde{\omega}_2 + \cdots + [X]\vec{V}_k\tilde{\omega}_k \tag{2.12}$$

2.2 SU^2 (Stanford-University-Unstructured) - Open Source Flow Solver

SU^2 suite is an open-source collection of software tools written in C++ for performing Partial Differential Equation (PDE) analysis and solving PDE-constrained optimization problems. The tool-set is designed with computational fluid dynamics and aerodynamic shape optimization in mind, but it is extensible (and has been extended) to treat arbitrary sets of governing equations such as electrodynamics, chemically reacting flows, and many others [7].

2.2.1 Governing Equations

SU^2 capable of solving Reynolds-averaged Navier-Stokes (RANS) equations for both incompressible and compressible regimes. Particularly PDE system of a physical problem is modeled as follows:

$$\partial_t U + \nabla \cdot \vec{F}^c - \nabla \cdot \vec{F}^v = Q \tag{2.13}$$

$$\begin{aligned}
&U : \; Vector\ of\ state\ variables \\
&\vec{F}^c(U) : \; Convective\ fluxes \\
&\vec{F}^v(U) : \; Viscous\ fluxes \\
&Q(U) : \; Source\ term
\end{aligned}$$

For the numerical solution of atmospheric flow field steady, compressible Navier-Stokes equations are used neglecting the gravitational effect for viscous flow. For this case state variables are, $U = (\rho, \rho u, \rho v, \rho w, \rho E)^T$ where u, v, w velocity components in x, y, z directions , ρ is the density, and E is the total energy per unit mass [22].

$$\vec{F}^c_x = \begin{pmatrix} \rho u \\ \rho u^2 + P \\ \rho uv \\ \rho uw \\ \rho uH \end{pmatrix}, \vec{F}^c_y = \begin{pmatrix} \rho v \\ \rho vu \\ \rho v^2 + P \\ \rho vw \\ \rho vH \end{pmatrix}, \vec{F}^c_z = \begin{pmatrix} \rho w \\ \rho wu \\ \rho wv \\ \rho w^2 + P \\ \rho wH \end{pmatrix} \tag{2.14}$$

$$\vec{F}^v_x = \begin{pmatrix} \cdot \\ \tau_{xx} \\ \tau_{xy} \\ \tau_{xz} \\ V_j \tau_{xj} + \mu^*_{tot} C_p \partial_x T \end{pmatrix},$$

$$\vec{F}^v_y = \begin{pmatrix} \cdot \\ \tau_{yx} \\ \tau_{yy} \\ \tau_{yz} \\ V_j \tau_{yj} + \mu^*_{tot} C_p \partial_y T \end{pmatrix},$$

$$\vec{F}^v_z = \begin{pmatrix} \cdot \\ \tau_{zx} \\ \tau_{zy} \\ \tau_{zz} \\ V_j \tau_{zj} + \mu^*_{tot} C_p \partial_z T \end{pmatrix} \tag{2.15}$$

Where P is the static pressure, H is the fluid and τ_{ij} is the viscous stresses defined as $\tau_{ij} = \mu_{tot}(\partial_j V_i + \partial_i V_j - 2/3\delta_{ij} \nabla \cdot \vec{V}$ In the above equations C_p is the specific heat, T is the temperature and μ_{tot} is the total viscosity:

$$\mu_{tot} = \mu_{dyn} + \mu_{turb}, \quad \mu^*_{tot} = \frac{\mu_{dyn}}{Pr_{dyn}} + \frac{\mu_{turb}}{Pr_{turb}} \tag{2.16}$$

In this thesis, SU^2 computations are performed in the High Performance Computing cluster in METUWIND with parallel processing. Operating system of the cluster is Linux, and the version of the SU^2 flow solver is 4.2 "Cardinal" version. For the solutions of atmospheric flow field following boundary condition types are applied to the RANS solver SU^2:

- Inlet : Density, velocity magnitude and direction specified, used for inflow
- Outlet : Static pressure specified, used for outflow
- Far-field : Applied to the top of the domain

The following solver attributes are used for the atmospheric flow field solutions:

- Regime type: Incompressible
- Convergence acceleration technique : GMRES
- Convective numerical method : LAX-FRIEDRICH method with 2nd order limiter
- Turbulent convective numerical method : Scalar Upwind
- Convergence criteria: Cauchy method applied to drag function with $\epsilon = 10^{-5}$

2.3 Discretization of Computational Domain

In order to capture the terrain effects accurately the computational grid should be based on high resolution terrain data. Blocken listed in his 2007 article [4] basic requirements for the simulation of atmospheric boundary layer (ABL) flows as follows:

- A sufficiently high mesh resolution in the vertical direction (e.g. height of first cell < 1 m)
- Knowing the relationship between the equivalent sand-grain roughness height k_s and the corresponding aerodynamic roughness length y_0
- A horizontally homogeneous ABL flow in the upstream and downstream region of the domain

In this study the grid layers in the vertical direction (i.e. z-direction) has a resolution of $1m$ on the terrain surface, and stretches rapidly (Figure 2.1).

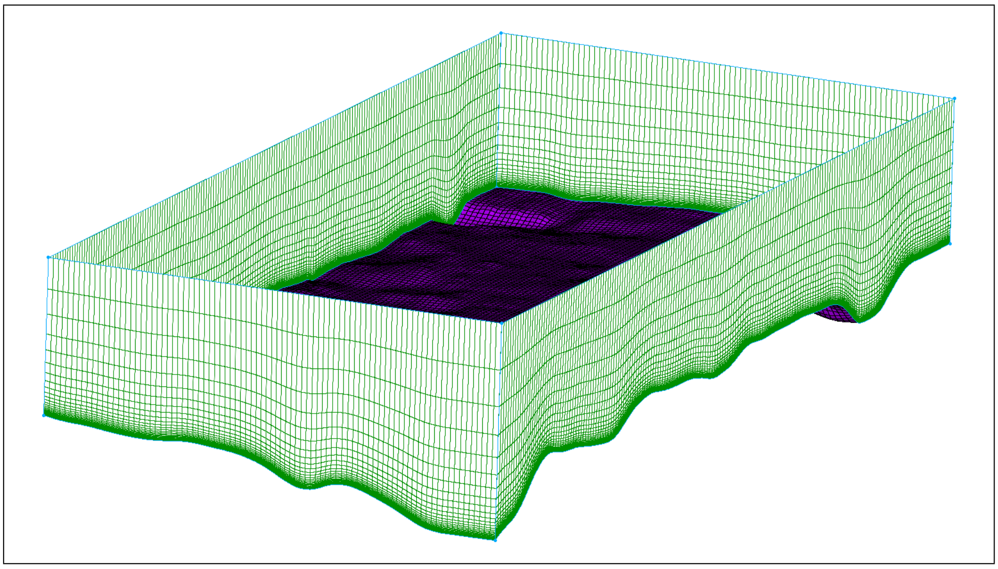

Figure 2.1: Flow field edge length contours in z-direction and its histogram

Neither roughness nor wall functions are not implemented in the SU^2 suite. Therefore item three is not valid for this right now. However, the first two items are successfully applied for our computational domain.

2.3.1 Smoothing and Extension of Terrain

Since SU^2 is not capable of providing spatially varying boundary conditions, an atmospheric boundary layer profile could not be imposed at the inflow boundaries. In order to have a realistic flow field computed within the solution domain, the domain boundaries are extended and the terrain surface is flattened in order to apply uniform inflow conditions at the extended boundaries. Such an extension allows the atmospheric boundary layers to develop naturally at the actual domain boundaries.

According to Mochida [18], the size of the computational domain should be related with the height single model building solved in that domain. The inlet, the lateral and top boundary should be set $5H$, where the H is the building height, the outlet boundary should be set at least $15H$. As this study is related with flow field solutions of complex terrain, there are not any building in the computational area. So, the height H is assumed to be the difference between the maximum altitude of the domain and the minimum altitude of the domain. In this study, the computational domain is extended about 5000 m in the azimuthal directions, which is about $10H$.

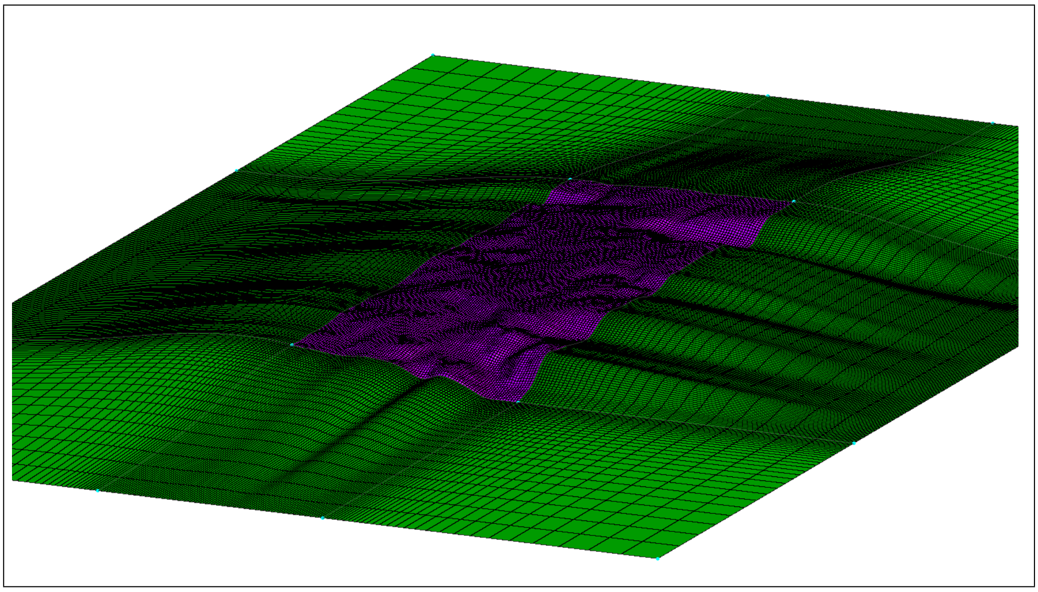

Figure 2.2: Smoothing and extension of the computational domain: Purple: Terrain surface over the wind farm, Green: Extended computational surface.

The wall surface of the computational domain is redesigned and improved by extending wall from the corners of the region of interest (Figure 2.2), and smoothing extended parts to the lowest altitude of the whole computational domain according to literature (Figure 2.3). With this improvement it is aimed to obtain ABL profile at the inlet of the central wall.

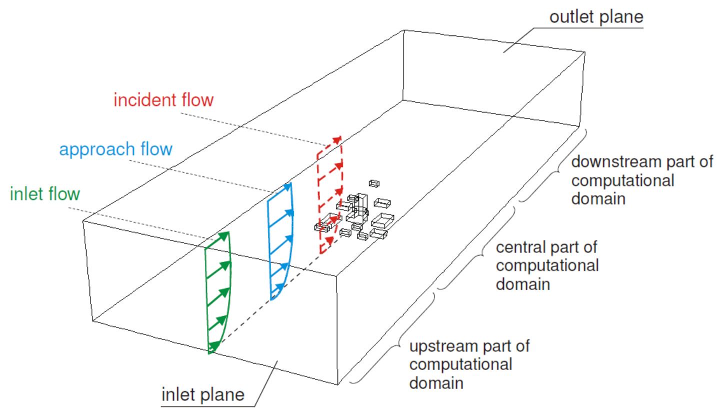

Figure 2.3: Extended computational domain – definition of inlet flow, approach flow and incident flow [4]

CHAPTER 3

RESULTS AND DISCUSSION

The results are presented in three main sections. The first one is dedicated to the reconstruction of 2D flow fields as a validation study. The pressure distribution over a NACA0012 airfoil is considered. This reconstruction is applied for two different cases including the reconstruction of existing data and the reconstruction of missing data. Then, reconstruction of pressure field in he computational domain is performed. The reconstruction of 3D atmospheric flow field are presented in the second section. Finally the predictions of the POD based current method are compared with WindSim predictions:

- Reconstruction of 2D flow fields around NACA0012 as a validation study
  - Reconstruction of C_p distribution on the airfoil with original data
  - Reconstruction of C_p distribution on the airfoil with missing data
  - Reconstruction of C_p distribution around the airfoil with missing data
- Reconstruction of atmospheric flow fields
- Comparison of the POD based current method and the WindSim software

3.1 Reconstruction of 2D Flow Fields

Before applying POD method to the reconstruction of atmospheric flow fields , using POD method for the reconstruction of the 2D pressure field around the airfoil is cheaper and easier in terms of computational cost and debugging and correction of the

POD code. Application of POD for the other flow fields can be possible, but pressure field is chosen for this study. Therefore, as a validation study POD is implemented on reconstruction of 2D pressure distribution around an airfoil. The purpose of the 2D validation is because this case is much smaller compared to the atmospheric flow field solutions, and observation and correction of the mistakes in the method is easier.

The pressure coefficient is the ratio of static pressure to the dynamic pressure (Equation 3.1):

$$C_{p_i} = 1 - (\frac{V_i}{V_\infty})^2 \tag{3.1}$$

$$V_\infty = \frac{M_\infty}{a_\infty} \tag{3.2}$$

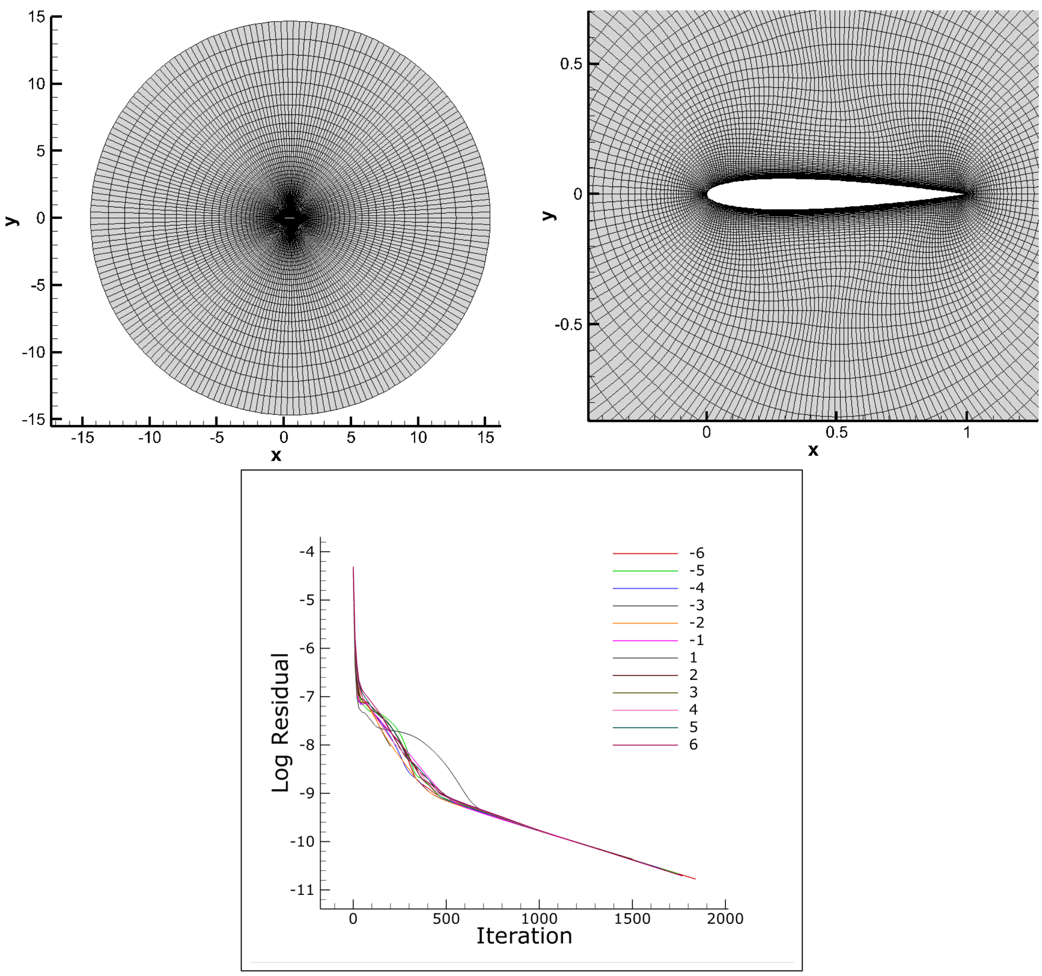

Figure 3.1: Computational grid and convergence of residuals with respect to angle of attack

The flow field around NACA0012 airfoil is discretized by a 198×78 size structural grid and the flow solutions are obtained for different angle of attack values at a fixed Mach number of $M_\infty = 0.2$ (Figure 3.1). A total of 12 different flow solutions are obtained for the angle of attack values ranging from of -6°to 6°. The following sets are considered for the solution snapshots of POD : 4 (-6° , -3° , 3° , 6°), 6 (-6° , -4° , -2° , 2° , 4° , 6°) and 12 (-6° , -5° , -4° , -3° , -2° , -1° , 1° , 2° , 3° , 4° , 5° and 6°). A validation case is also computed at 1.5° angle of attack.

3.1.1 Reconstruction of Airfoil Surface Pressure Distribution

Once the flow solutions at different angle of attacks are obtained for the NACA0012 profile, the data set required for POD , $[X]$, is created using 198 pressure coefficient values on the airfoil surface for 12 solutions (Equation 3.3):

$$[\mathbf{X}]_{\mathbf{198\times 12}} = \begin{array}{cc} \begin{array}{ccccc} \alpha_1 & \alpha_2 & \cdots & \cdots & \alpha_{12} \end{array} & \\ \begin{bmatrix} c_{P_{1,1}} & c_{P_{1,2}} & \cdots & \cdots & c_{P_{1,12}} \\ c_{P_{2,1}} & c_{P_{2,2}} & \cdots & \cdots & c_{P_{2,12}} \\ \vdots & \vdots & \vdots & \vdots & \vdots \\ c_{P_{198,1}} & c_{P_{198,2}} & \cdots & \cdots & c_{P_{198,12}} \end{bmatrix} & \begin{array}{l} \text{Node 1} \\ \text{Node 2} \\ \vdots \\ \text{Node 198} \end{array} \end{array} \tag{3.3}$$

$$[X]_{198\times 12} = [U]_{198\times 198}\,[S]_{198\times 12}\,[V]^T_{12\times 12} \tag{3.4}$$

$$\tilde{\vec{X}}_{198\times 1} = [U]_{198\times k}\,\vec{\omega}_{k\times 1} \tag{3.5}$$

$$k:\ number\ of\ dominant\ mods$$

Based on this data set firstly, the reconstruction of the pressure distribution on the airfoil surface for the existing data ($\alpha = 3°$) case is performed by Equation 3.4, Equation 3.5. In this case there is no need to work with the correlation matrix because the data set size is small enough for the memory size of the desktop computer. Based on the eigenvalues and the POD coefficients computed, the dominance of the first POD

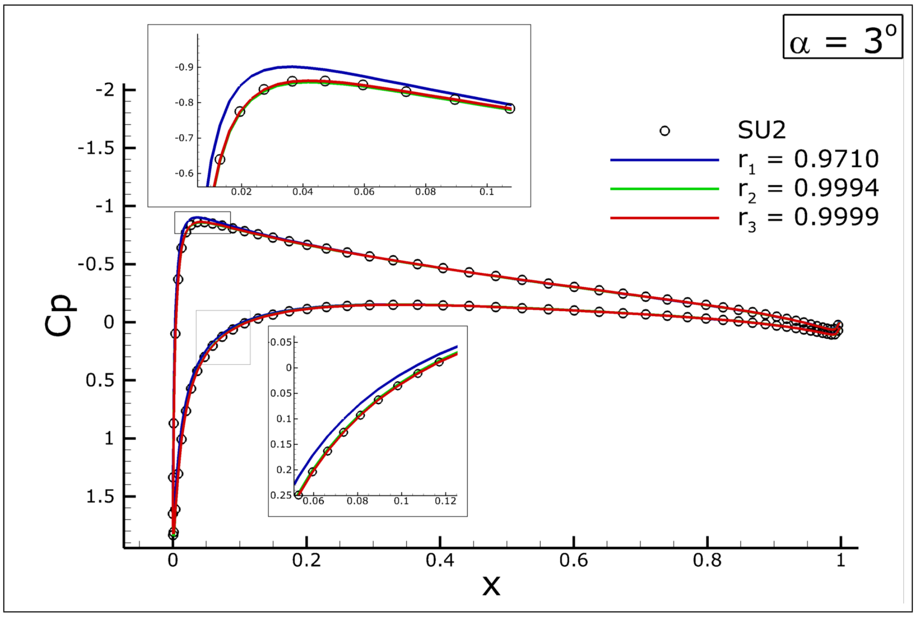

Figure 3.2: Reconstruction of existing C_p distribution at $\alpha = 3°$, $M = 0.2$

mod is ($r_1 = 0.9710$), the dominance of first 2 mods is ($r_2 = 0.9994$) and dominance of first 3 mods is ($r_3 = 0.9999$).

The surface pressure coefficients reconstructed at 3° angle of attack by the present POD method using 1, 2, and 3 dominant modes are compared with SU^2 solutions in Figure 3.2. As shown, the reconstruction with 2 and more modes provides an acceptable accuracy.

3.1.2 Reconstruction of Airfoil Surface Pressure Distribution at an Arbitrary Angle of Attack

Following the reconstruction of an existing data set, the present POD method is now applied for the reconstruction of surface pressure distribution at an arbitrary angle of attack which does not exist in the data set $[X]$. The validation angle of attack is taken as 1.5° .

The POD coefficients needed for the reconstruction are obtained by interpolation (Figure 3.3). Then, Equation 3.5 is modified for the reconstruction of arbitrary angle of

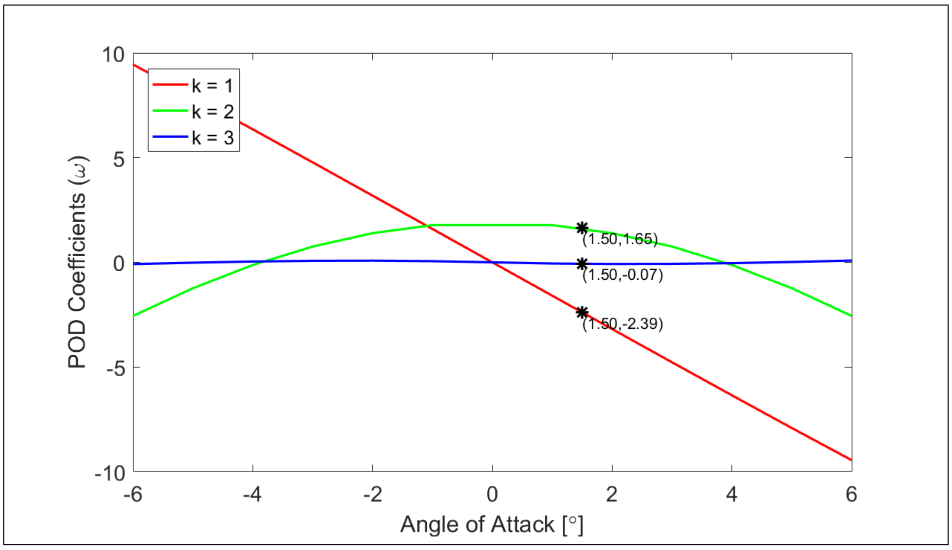

Figure 3.3: Interpolation of POD coefficients ω for an arbitrary angle of attack

attack solution, as follows:

$$\tilde{\vec{X}}_{198\times 1} = [U]_{198\times k}\, \tilde{\vec{\omega}}_{k\times 1} \tag{3.6}$$

where $\tilde{\vec{\omega}}$ is the interpolated POD coefficients at the reconstruction angle of attack, 1.5° . Using the $\tilde{\vec{\omega}}$ values, the reconstruction of surface pressure at 1.5° angle of attack solution is obtained, and it is compared with the numerical solution at $\alpha = 1.5°$ (Figures 3.4, 3.3). It is seen from the figure that the reconstructed C_p distribution by the present POD method using 2 or more dominant modes are in good agreement with the exact C_p distribution.

Next, the reconstruction of the pressure distribution with different the number of data sets in $[X]$, that is, the number of flow solutions is investigated. The data set, $[X]$, is created by using 4 $([X]_{198\times 4})$, 6 $([X]_{198\times 6})$ and 12 $([X]_{198\times 12})$ solutions. Then the surface pressure distribution at $\alpha = 1.5°$, is again reconstructed. The results are compared with the SU^2 solution in Figure 3.5. It is seen that even a coarse set of 6 solutions provides enough information through the POD modes to reconstruct an unknown surface pressure distribution.

In the next section, the reconstruction of field variables will be performed in the same manner. The data sets will be formed by solution variables computed at all the grid points instead of boundary points as in the case of surface pressures.

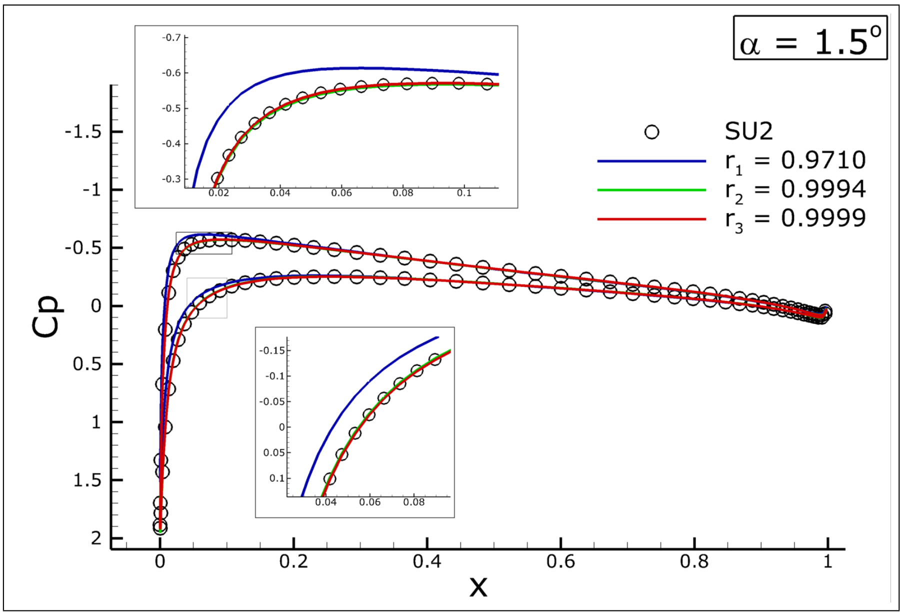

Figure 3.4: Reconstruction of C_p distribution for at $\alpha = 1.5^\circ$, $M = 0.2$

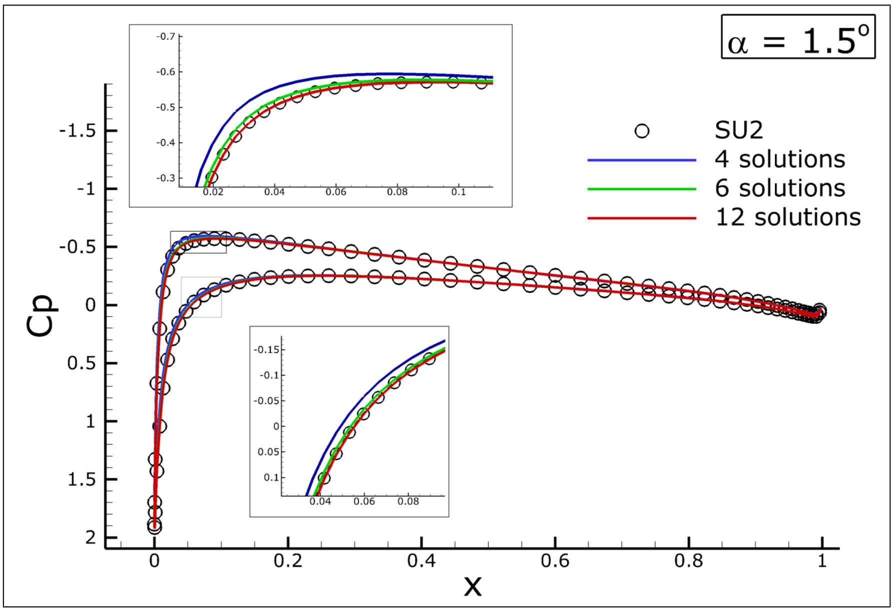

Figure 3.5: Reconstruction of C_p distribution for at $\alpha = 1.5^\circ$, $M = 0.2$ with respect to data set size

3.1.3 Reconstruction of 2D Pressure Fields

In the previous case, the method is applied for only the reconstruction of the pressure distribution on the airfoil surface. Whereas in this case the reconstruction of the whole pressure field in the computational domain is aimed. For the reconstruction, the numerical solutions obtained earlier are used. Reconstruction of the pressure distribution is similarly performed at 1.5° angle of attack.

12 data sets, each of which consists of 15444 (198 × 78) nodal pressure values are employed (Equation 3.7). Since the size of the current data sets is large, unlike the previous case, instead of performing the SVD of data set $[X]$, the SVD of the correlation matrix $[C] = [X]^T\ [X]$ is performed and the corresponding mode vectors and the POD coefficients are obtained. The dominance of the first POD mode is found to be $r_1 = 0.99957$, the first 2 POD mods is $r_2 = 0.999993$ and , the first 3 POD mods is $r_3 = 0.999999$.

$$[X]_{198*78\times12} = \begin{bmatrix} c_{P_{1*1,1}} & c_{P_{1*1,2}} & \cdots & \cdots & c_{P_{1*1,12}} \\ c_{P_{2*1,1}} & c_{P_{2*1,2}} & \cdots & \cdots & c_{P_{2*1,12}} \\ \vdots & \vdots & \vdots & \vdots & \vdots \\ c_{P_{198*1,1}} & c_{P_{198*1,2}} & \cdots & \cdots & c_{P_{198*1,12}} \\ c_{P_{1*2,1}} & c_{P_{1*2,2}} & \cdots & \cdots & c_{P_{1*2,12}} \\ c_{P_{2*2,1}} & c_{P_{2*2,2}} & \cdots & \cdots & c_{P_{2*2,12}} \\ \vdots & \vdots & \vdots & \vdots & \vdots \\ c_{P_{198*2,1}} & c_{P_{198*2,2}} & \cdots & \cdots & c_{P_{198*2,12}} \\ \vdots & \vdots & \vdots & \vdots & \vdots \\ c_{P_{1*78,1}} & c_{P_{1*78,2}} & \cdots & \cdots & c_{P_{1*78,12}} \\ c_{P_{2*78,1}} & c_{P_{2*78,2}} & \cdots & \cdots & c_{P_{2*78,12}} \\ \vdots & \vdots & \vdots & \vdots & \vdots \\ c_{P_{198*78,1}} & c_{P_{198*78,2}} & \cdots & \cdots & c_{P_{198*78,12}} \end{bmatrix} \tag{3.7}$$

The pressure field at 1.5° angle of attack reconstructed by using 1,2 and 3 dominant mods are shown and compared to the flow solution in Figure 3.6. As seen in the figures, although the POD reconstruction with 1 mod captures the main features of

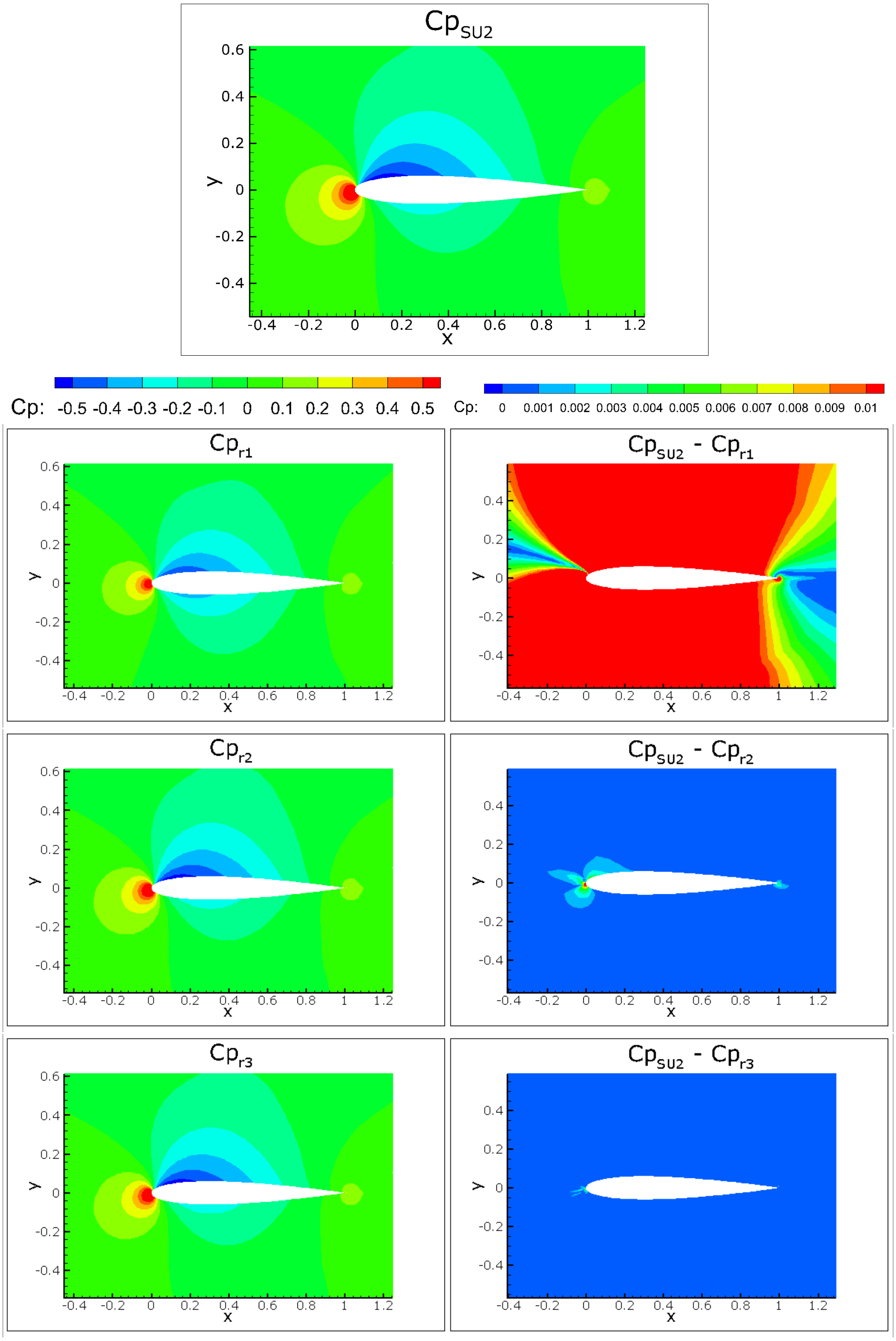

Figure 3.6: Reconstruction of pressure field using increasing number of POD modes at $\alpha = 1.5°$, $M = 0.2$

the pressure distribution in the flow field, it relatively has a large error. On the other hand, the reconstruction of the pressure field with 3 modes has an RMS error value of 0.003.

As shown in this validation cases, the POD based methodology developed can successfully be used in the reconstruction of flow fields.

3.2 Reconstruction of Atmospheric Flow Fields

The main goal of this study is the reconstruction of the atmospheric flow fields over wind farms based on the fictitious flow fields computed by SU^2 and the statistical wind data at one or more locations within the wind farm, which should ideally be obtained from a mat-mast installation. However, in order to assess the accuracy of the reconstructed flow fields, the wind data to be used in the reconstruction will be extracted from a computed flow field, which is excluded from the data set used in the POD method. The reconstructed flow fields will then be compared with the computed flow field to assess the error. An operational wind farm location in Mut-Mersin region in Turkey will be considered in the study.

In this section, the results obtained are presented in the following order:

- Flow Fields Computed by SU^2
  - Grid Generation
  - Boundary Conditions
  - Parallel Performance
- Reconstructed wind fields by the present POD based Method

3.2.1 Flow Fields Computed by SU^2

The fictitious flow fields over a wind farm are simulated with the open-source Navier-Stokes solver SU^2. Computations are performed in a parallel computing environment.

High resolution terrain elevation data are used in the generation of terrain fitted computational grids. Computed flow fields are also compared against the flow solutions predicted by the weather prediction software WRF.

3.2.1.1 Grid Generation

For an accurate computation of turbulent flow fields, high resolution computational grids are needed. For this purpose, high resolution digital elevation model (DEM) data are obtained from the ASTER-GDEM database having 1 arc-second resolution on the ground. The DEM data for the Mut region in Mersin/Turkey is obtained from Aster-GDEM for a domain of 7km x 3.5km size with 38 m resolution. The surface grid over the terrain is discretized by structured grid of 186×87 size, which provides around 40m resolution (Figure 3.7). The atmospheric flow field in the vertical direction is discretized with 30 nodes. The grid distribution in the vertical direction is stretched starting off with the first grid size of $1m$ on the terrain surface. Then computational grid is created over Mut topography which includes over 1 million structural elements with smoothed and extended topography (Figure 3.8).

3.2.1.2 Flow Models and Boundary Conditions

SU^2 software has a selection of flow models and solution algorithms (Figure 3.9a). In this study atmosperic flows are assumed to be turbulent and Spalart-Allmaras turbulence model is used. The convective fluxes is evaluated with 2nd order LAX-FRIEDRICH method with limiters. The solution of linear system of equations is obtaned with the GMRES algorithm (Figure 3.9b).

Similarly, SU^2 software has quite a few types of boundary condition, which can be easily implemented. Boundary names are to be listed in the grid input file ".su2" with markers. The selected boundary condition is then assigned to the marker name in the configuration file ".cfg" (Figure 3.9c).

For the solution of atmospheric flow fields the following boundary conditions are applied:

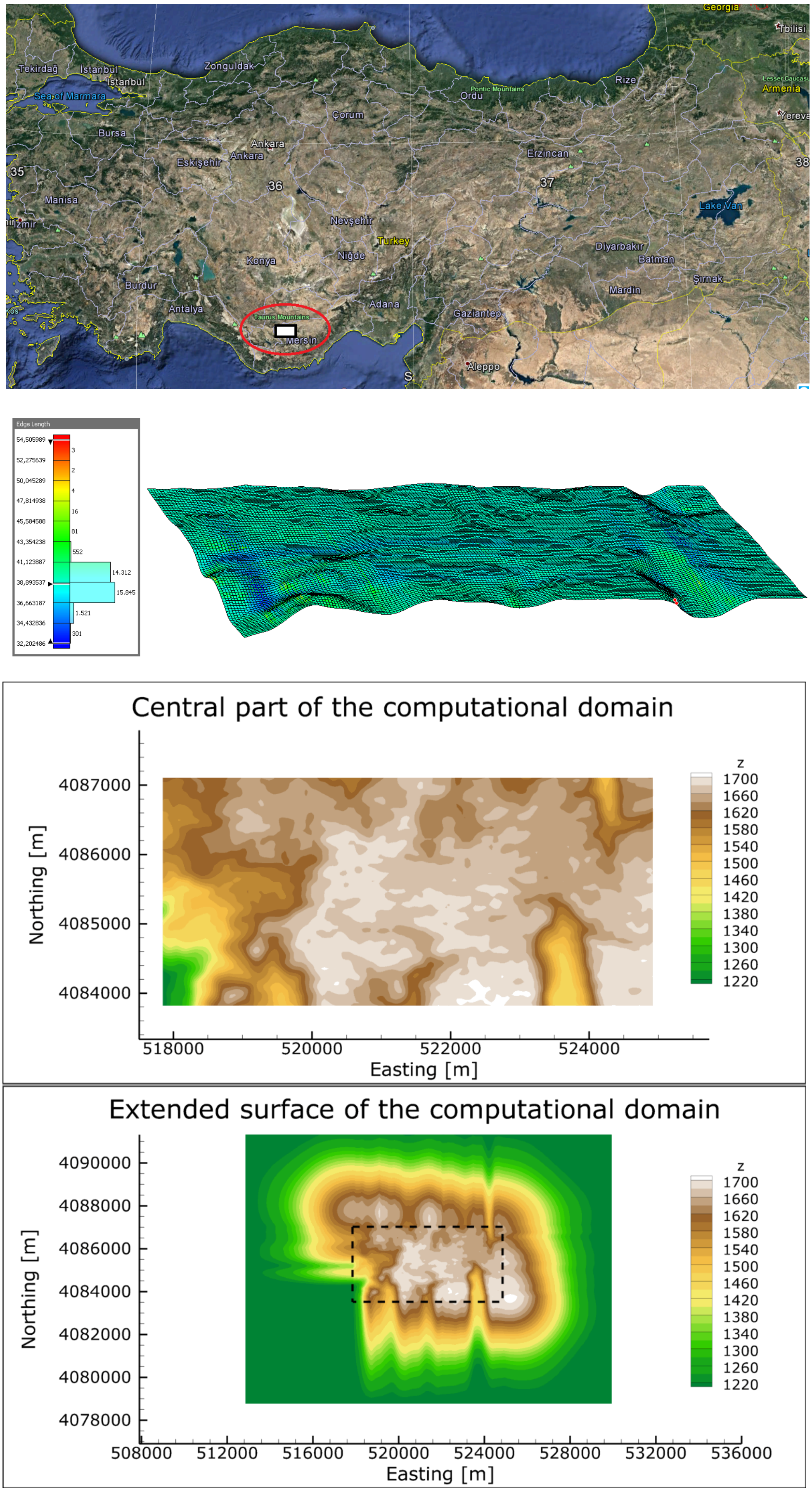

Figure 3.7: Interested solution region, the wall surface grid and elevation maps of central region and extended region of Mut region in Mersin/Turkey

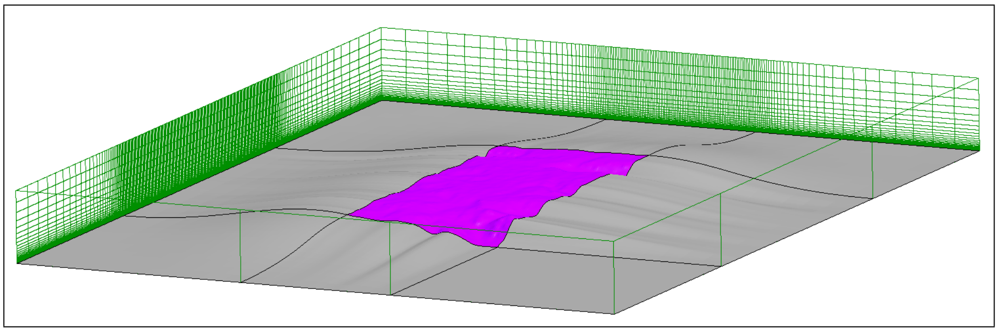

Figure 3.8: Computational domain of Mut region in Mersin/Turkey

- Inflow/Outflow
- No-slip wall
- Far-field

In SU^2 software suite, inflow and outflow boundary conditions are created based on characteristic information, meaning that only certain flow quantities can be specified as the inlet and outlet condition. Inflow is specified as "inlet" condition with specifying the velocity vector and density at the inflow locations. Outflow is specified as "outlet" condition, in which free stream pressure is given. Being a Navier-Stokes solver, SU^2 implements no-slip wall boundary conditions for viscous flows. The far-field boundary condition applies uniform flow conditions at the boundaries, which is imposed before the iterative solution process begins. The inflow-outflow and wall surfaces are shown in the Figure 3.10.

As a validation and verification study of SU^2 for the simulation of atmospheric flow fields , an SU^2 solution is compared with the WRF solution. a probe location is chosen at central part of the computational domain, then the at that point. One challenge for this verification and validation of SU^2 with WRF is difference in terrain and grid resolutions. In addition, WRF uses eta (η) coordinate ssytem to represent the height while SU^2 uses the distance in meters. This challenge is presented in detail by Leblebici, Ahmet and Tuncer [14]. The difficulty is overcome by interpolating ans shifting WRF nodes into the high resolution CFD domain. From the results they obtained for Mut location, one-point solution of WRF is interpolated into the CFD domain. The WRF solution is obtained in Mut region under fixed, time independent boundary conditions (Figure 3.11). The SU^2 solution is similarly obtained for the average wind direction

```
%%%%%%%%%%%%%%%%%%%%%%%%%%%%%%%%%%%%%%%%%%%%%%%%%%%%%%%%%%%%%%%%%%%%%%%%%%%%%%%%

% ------------- DIRECT, ADJOINT, AND LINEARIZED PROBLEM DEFINITION ------------%
%
% Physical governing equations (EULER, NAVIER_STOKES)
% Euler: inviscid, Navier-Stokes: viscous
PHYSICAL_PROBLEM= NAVIER_STOKES
%
% Specify turbulence model (NONE, SA, SA_NEG, SST)
% NONE: Laminar, SA: Spalart-Allmaras
KIND_TURB_MODEL= SA

% Mathematical problem (DIRECT, CONTINUOUS_ADJOINT)
MATH_PROBLEM= DIRECT
```

(a)

```
% -------------------- FLOW NUMERICAL METHOD DEFINITION -----------------------%
%
% Convective numerical method (JST, LAX-FRIEDRICH, CUSP, ROE, AUSM, HLLC,
%                              TURKEL_PREC, MSW)
CONV_NUM_METHOD_FLOW= LAX-FRIEDRICH
%
% Spatial numerical order integration (1ST_ORDER, 2ND_ORDER, 2ND_ORDER_LIMITER)
SPATIAL_ORDER_FLOW= 2ND_ORDER_LIMITER
%
% Slope limiter (VENKATAKRISHNAN, BARTH_JESPERSEN)
SLOPE_LIMITER_FLOW= VENKATAKRISHNAN
% Coefficient for the limiter (smooth regions)
LIMITER_COEFF= 0.3
%
% Linear solver or smoother for implicit formulations
% (BCGSTAB, FGMRES, SMOOTHER_JACOBI,
%  SMOOTHER_ILU0, SMOOTHER_LUSGS,
%  SMOOTHER_LINELET)
LINEAR_SOLVER= FGMRES
```

(b)

```
% -------------------- BOUNDARY CONDITION DEFINITION -------------------------%
%
% Navier-Stokes (no-slip), constant heat flux wall  marker(s) (NONE = no marker)
MARKER_HEATFLUX= ( wall, 0.0 )
% Far-field boundary marker(s) (NONE = no marker)
MARKER_FAR= ( top )
% Symmetry boundary marker(s) (NONE = no marker)
MARKER_SYM= ( sym )
% Inlet boundary marker(s) (NONE = no marker)
MARKER_INLET= ( xm, 1.073244444, 9, 1.0, 0, 0, xm_ym, 1.073244444, 9, 1.0, 0, 0,...
% Outlet boundary marker(s) (NONE = no marker)
MARKER_OUTLET= (  xp, 92425.02, xp_ym, 92425.02,xp_yp,92425.02 )
```

(c)

Figure 3.9: SU^2 solver options: a)-flux splitting algorithms and linear solvers, b)-boundary conditions, c)- configuration ".cfg" file

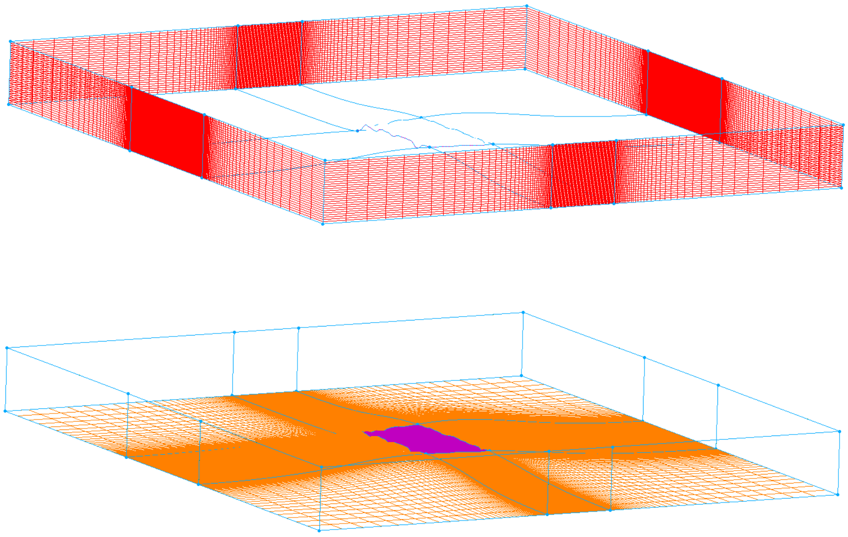

Figure 3.10: Inflow-uutflow and wall boundaries

and the average wind speed applied at the extended inflow boundaries. The mean wind direction is $19.468\ ^\circ$ sector, and the mean wind speed is $9.4783 m/s$. The flow solutions with SU^2 are obtained for the following inflow conditions:

- Direction = 20 °
- Wind Speed = 9 m/s

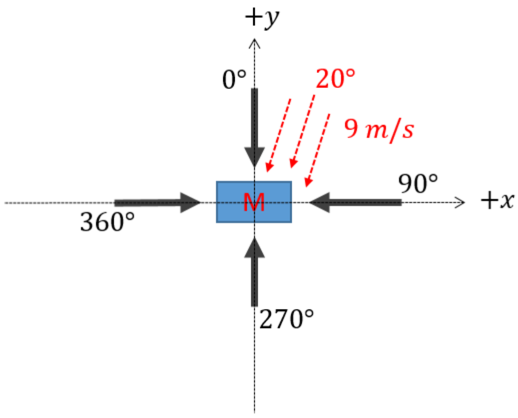

The SU^2 and the WRF solutions are in agreement at high altitudes as expected (Figure 3.12). The object of this comparison is to show that SU2 is capable of solving atmospheric flow field with given conditions. As the inlet velocity $9m/s$ is chosen, which is the WRF mean velocity at the 2200 m altitude. Then the constant velocity profile is turned out to be boundary layer,and the wind speed remained constant at the top of the domain. As observed in the figure an atmospheric boundary layer profile is predicted in the SU^2 solution.

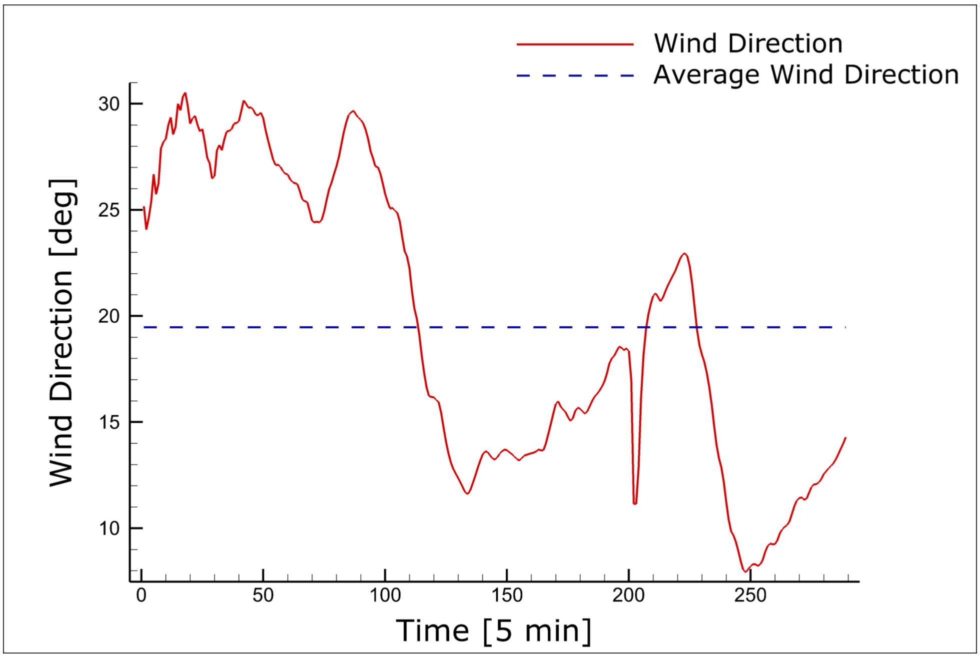

(a) Wind direction at 2200 meter altitude vs. Time

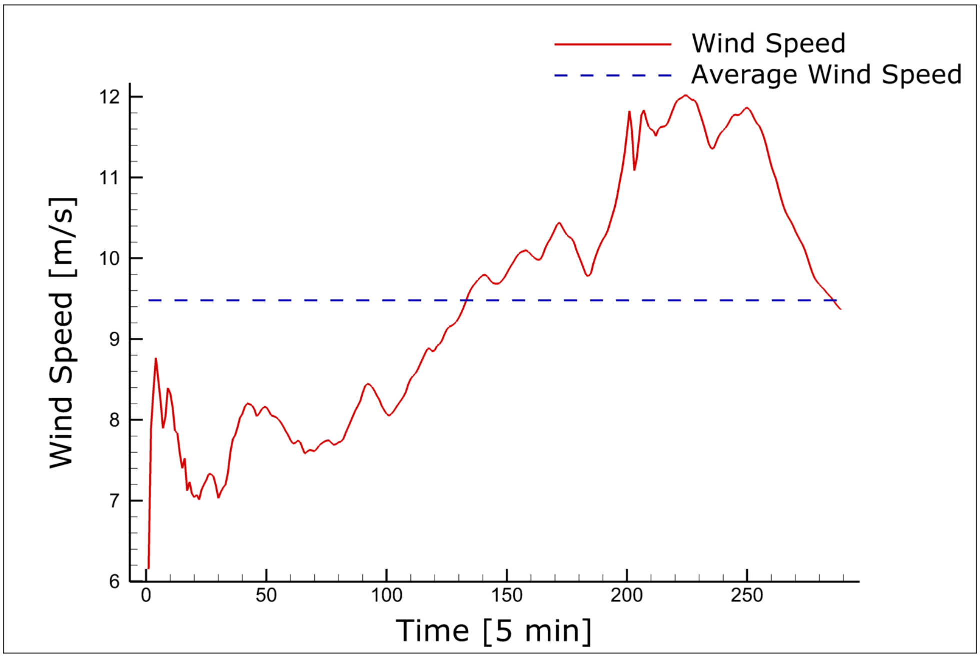

(b) Wind speed at 2200 meter altitude vs. Time

Figure 3.11: WRF Solution for 1-day with $\delta t = 5min$

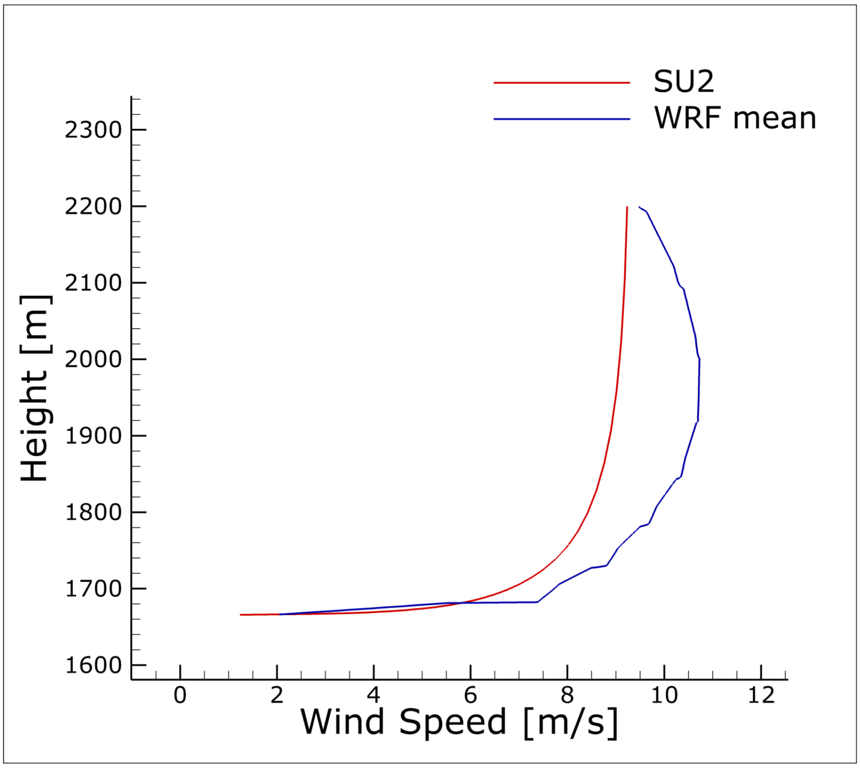

(a)

Figure 3.12: SU2 and WRF wind speed comparisons

3.2.1.3 Parallel Performance

The open source flow solver SU^2 has a parallel computing capability based on domain decomposition. Atmospheric flow field solutions require big size domains due to their interested wall surface covers wide area. The computational domain has over 1 million cells, then the computational time for this domain with single processor taking too much time considering 12-sector solutions. To reduce the computation and debugging time, built-in parallel option of SU^2 suite is used for the simulations. Parallel computations not only applicable for the clusters but also for the PCs but for this study only High Performance Computing (HPC) cluster is used. The simulations were run in METUWIND HPC lab which has 512 core capacity from 8 node includes 64 core each. The solutions are compared in terms of single core, 2 cores, 4 cores, 8 cores, 16 cores, 32 cores and 64 cores. Speed-up graph is created for 100 iterations with same conditions (Table 3.1), (Figure 3.13).

As grid of the Mut region has small boundaries at the corners of the domain, which

Table 3.1: SU^2 Parallel Performance

Number of cores	**Computation Time for 1 Iteration [sec]**	**Total Time for 100 Iterations [sec]**	**Speed Up**
1	15.63	1585.76	1
2	9.18	946.65	1.591
4	4.60	484.75	3.313
8	2.50	283.20	7.015
16	1.27	139.88	11.860
32	0.86	99.68	19.912
64	0.54	69.84	23.181

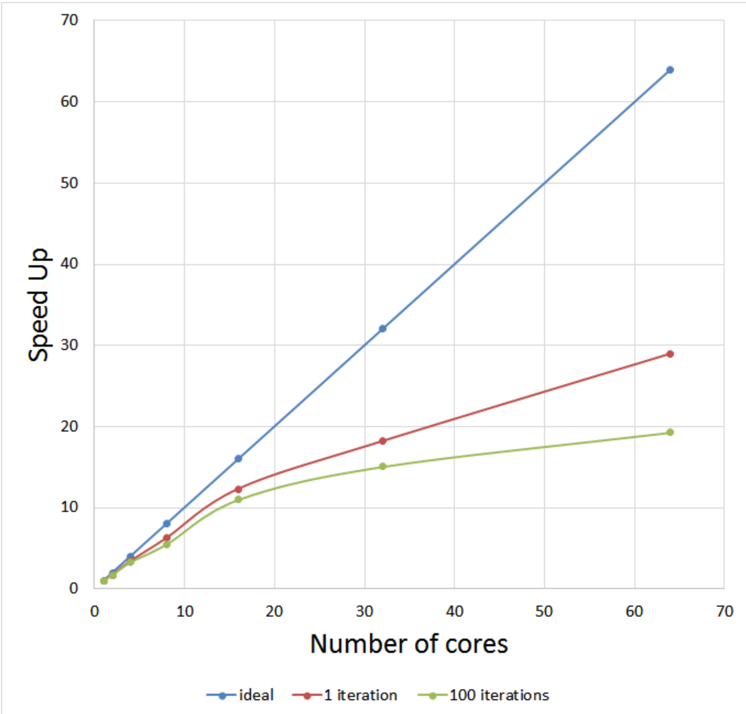

Figure 3.13: SU^2 parallel speed-up

has 195 elements, it is thought that those corner boundaries limits the parallel performance. Communication of those cells is choking the data transfer like a bottle neck. Even though computation is finished, the communication is still continues. Therefore performance is not risen well enough for the core number larger than 16 for this grid.

3.2.2 POD Based Reconstruction of Flow Fields

12-sector numerical flow field solutions are obtained from SU^2 flow solver with steady state conditions. The central part of the computational domain is extracted

Table 3.2: Z axis cuts and corresponding vertical distances

k [node number in z-direction]	**Node Wall Distance [m]**
1	10
2	20
3	30
4	40
5	50
6	60
7	70
8	80
9	90
10	100
11	150
12	200
13	250
14	300

into the new domain, which is constructed from the ground level up to 300 meters altitude. The new reconstruction domain has $88 \times 187 \times 14$ resolution in the i,j and k directions. The reason of the extraction is because the central part of the computational domain is our interested area, so, there is no need to apply POD method those smoothed and extended parts. By means of this extraction total node number is reduced from around 1 million (Figure 3.14a) to 230 thousand (Figure 3.14b). Additionally, this extraction and transformation decreases the computer memory for the calculation of POD method also the computation time.

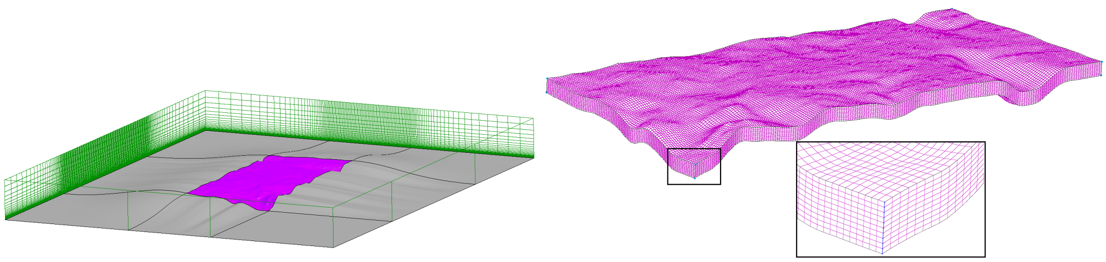

(a) Real Computational Domain

(b) Extracted Domain

Figure 3.14: Computational domain of size $244 \times 145 \times 30$ vs. Reduced domain of size $88 \times 187 \times 14$ used in reconstruction

The numerical solutions of atmospheric flow fields for all 12 different sectors, are transferred to the smaller domain with 230 thousand nodes, and the POD based reconstruction method is applied to the solution on the smaller grid. In the reconstruction process, the data set and the corresponding correlation matrix $[C] = [X]^T \times [X]$ are created. The data set $[X]$ is created in terms of the wind direction and the wind speed only(Equation 3.8).

$$[X]_{460768\times 12} = \begin{bmatrix} dir_{1,1} & dir_{1,2} & \cdots & \cdots & dir_{1,12} \\ dir_{2,1} & dir_{2,2} & \cdots & \cdots & dir_{2,12} \\ \vdots & \vdots & \vdots & \vdots & \vdots \\ dir_{230384,1} & dir_{230384,2} & \cdots & \cdots & dir_{230384,12} \\ V_{1,1} & V_{1,2} & \cdots & \cdots & V_{1,12} \\ V_{2,1} & V_{2,2} & \cdots & \cdots & V_{2,12} \\ \vdots & \vdots & \vdots & \vdots & \vdots \\ V_{230384,1} & V_{230384,2} & \cdots & \cdots & V_{230384,12} \end{bmatrix} \tag{3.8}$$

dir: Wind direction

V: Wind Speed

Flow variables are written side by side for each solution and one under the other for each node. Ones a variable completed, the next line starts with new variable. After constructing the matrix $[X]_{460768\times 12}$, correlation matrix $[C]_{12\times 12}$ is obtained by just simple matrix multiplication. Then POD modes, eigenvectors and eigenvalues $\phi_i, \lambda_i,\ i = 1, 2, ..., 12$, of the correlation matrix are calculated. Dominance ,r_m, of the modes are nothing but the ratio of the Euclidian Norm of the m number of eigenvalues and whole eigenvalues. The dominance of modes are altering with the number of solutions applied on POD method (Table (3.3)). As the number of solution increasing the difference between real solution and POD approximation is getting smaller. For a better approximation, the dominance value, r_m, of the m number of POD modes should be bigger than 0.95, which results in less than 5 % error for that number of solutions. Finally, data set $[X]$ is created by 12 different fictitious sectoral solutions, and the number of dominant used for the reconstruction is selected as 3 according to the dominance values.

Table 3.3: Dominance of the POD modes as a function of number of solutions in the dataq set

Number of solutions	**Number of dominant modes**	**Dominance**
4	1	0.84812
4	2	0.99999
6	1	0.83668
6	2	0.99999
12	1	0.96259
12	2	0.99998
12	3	0.99999

Mostly the maximum velocity difference between POD reconstruction and SU^2 solution is 1 m/s which occurs at the most complex part of the region. Also, the relative error is decreasing at middle parts of the computational domain because the one point used for the reconstruction is located at the middle part of the computational domain. The more near the reconstruction point means the more accurate approximation around that point. In order to see the POD method accuracy, POD results are extracted through the z axis. Slices are taken at 30m, 60m and 100m height above from the ground level. The comparison is done by vector fields of SU^2 and POD results, and SU^2 wind speed contour vs. POD wind speed relative error distribution (Figures 3.15) It is obvious that flow near the wall has low wind speed, once the altitude increases the flow velocity also increases. At the high altitude of the domain velocity contour is getting red, it means the flow velocity is getting closer to the free stream velocity 9 m/s. It can be said that from the figures the flow characteristic and dominant features ,such as velocity magnitude and direction, are reconstructed successfully. The POD reconstruction is obtained wind directions and wind speed properly. In a wide range of domain, POD method results have less than 10 % error.

At the upper parts of the domain, the velocity gradient is getting smaller due to the ABL profile and complexity is getting disappeared. Thus, the POD reconstruction at the upper parts are much accurate than the results at near the ground level.

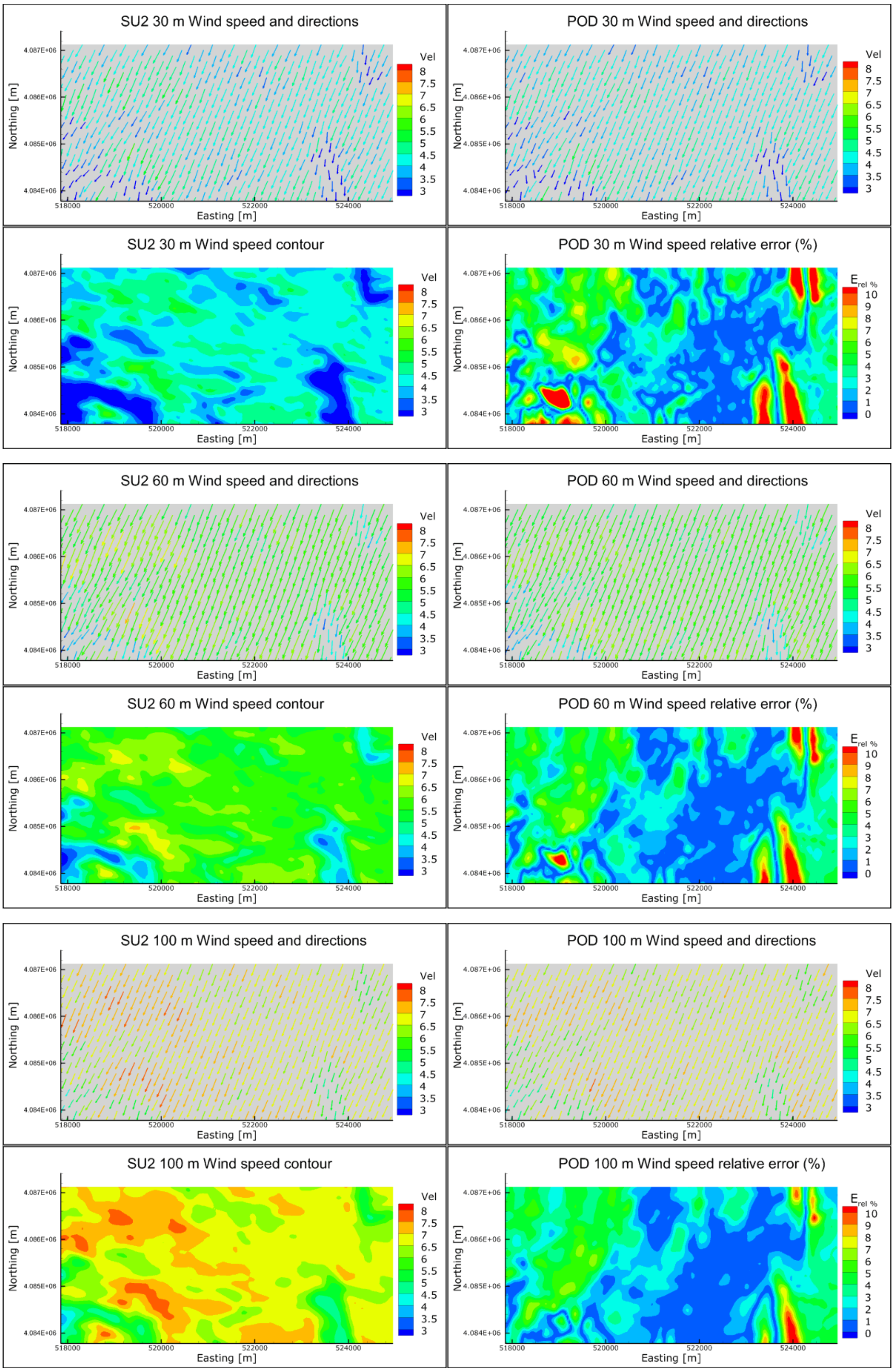

Figure 3.15: Comparison of reconstructed velocity fields with SU^2 solution at 30m, 60m and 100.

3.3 Comparison with WindSim Predictions

WindSim is a commercial tool used mainly for estimation of annual energy production (AEP) and micro-siting of wind turbines. WindSim takes the digital elevation map of a region of interest as an input. It then solves sectoral flow field over the domain. The input file (terrain digital elevation data) is obtained from ASTER-GDEM database and roughness data obtained from Corine database for the Mut/Mersin region, and they are imported to the WindSim software (Figure 3.16). It produces wind resource maps and AEP estimations as an output.

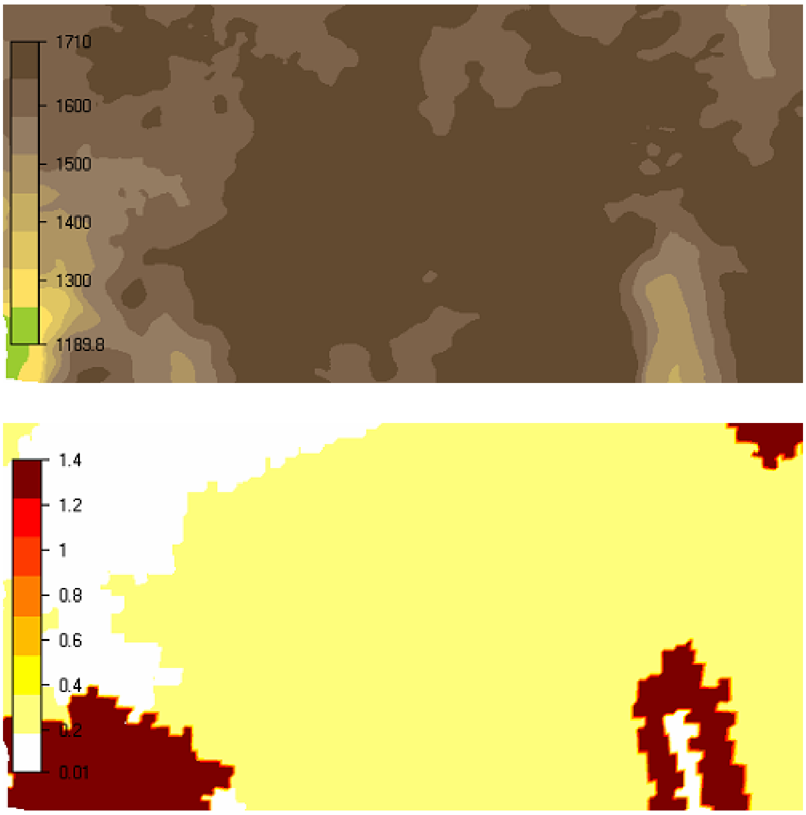

Figure 3.16: Digital terrain model - elevation (m) and roughness height (m), WindSim

The computational domain for WindSim is constructed with 30 layers in the vertical direction. A stretching grid extends 1000.0 (m) above the ground (Figure 3.17), (Table 3.4).

Table 3.4: Distribution of the first 10 nodes in z-direction

-	**1**	**2**	**3**	**4**	**5**	**6**	**7**	**8**	**9**	**10**
z-dist. max (m)	3.0	10.0	18.9	29.7	42.3	56.8	73.2	91.5	111.7	133.8
z-dist. min (m)	4.6	15.2	28.8	45.1	64.3	86.4	111.4	139.2	169.8	203.3

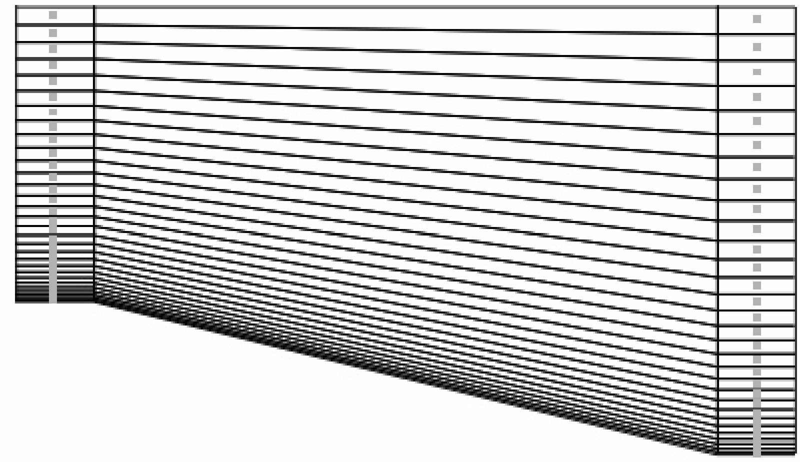

Figure 3.17: Digital terrain model - grid (z), WindSim

The wind fields are computed for 12 sectors. Height of the boundary layer is taken as 500 meters, and the free stream wind speed above the boundary layer is taken as $9m/s$. For the top boundary condition fixed pressure is selected. The free stream density is taken as $1.073kg/m^3$ and the turbulence model is chosen as the standard k-epsilon model. Calculations are performed until the residual drops down to 10^{-3}. The sector solutions are obtained for 12 different wind directions in terms of 0° , 30° , 60° , ..., 300° and 330° . Some of the wind field at 60 meter above the ground are shown and compared against the SU^2 solutions in Figures 3.18, 3.19, 3.20, and 3.21. As shown the wind speeds are predicted higher in WindSim predictions.

Since WindSim has an internal flow solver, the POD reconstruction is now applied with the WindSim sectoral solutions. While the sectoral average of the wind speed obtained by WindSim solutions are in good agreement with SU^2 solutions, there are significant wind speed differences at the 180 and 270 degree sector solutions as shown in Figure 3.22. It is observed that the wind magnitude in the WindSim solutions turns out to be significantly larger than the SU^2 solutions at the same altitude with the same boundary conditions. At some locations, the wind speed is larger than the free stream wind speed 9 m/s.

WindSim requires time series data from a met-mast to create resource maps. Since the field measurement data is not available, the time series data is provided from the SU^2 solution. A point 60 meter above the ground at the middle of the solution domain is selected to act like a MET-MAST, and it is the same point applied to POD

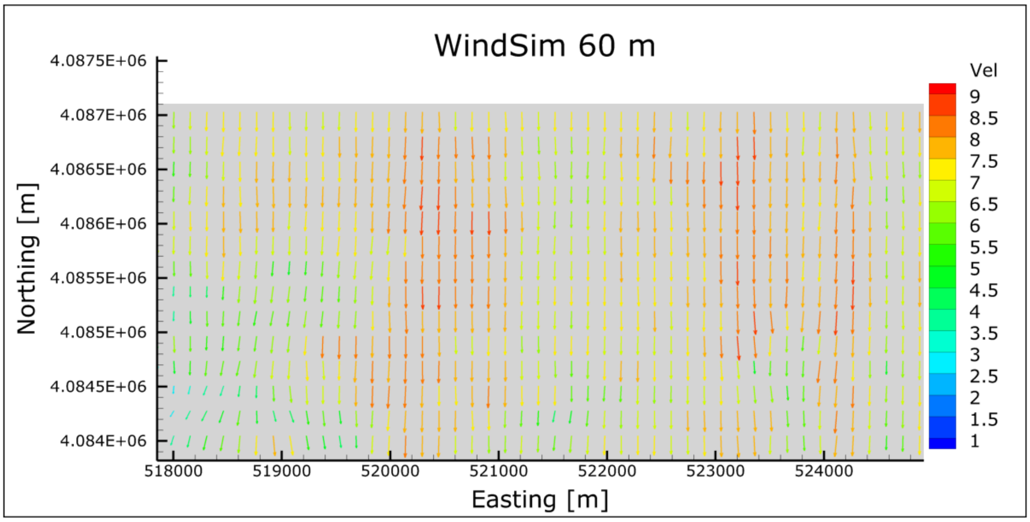

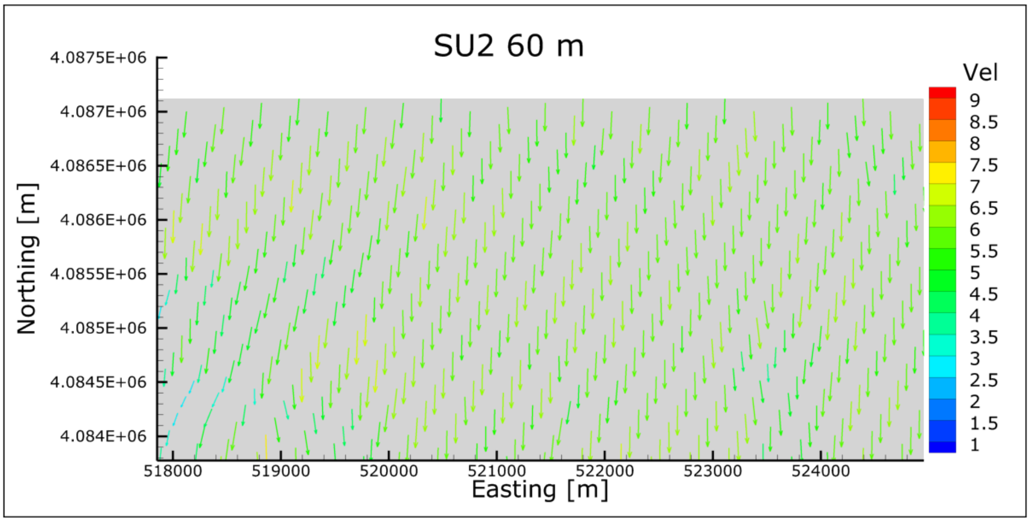

Figure 3.18: 0° sector solution comparison of WindSim and SU^2 at 60m above ground level

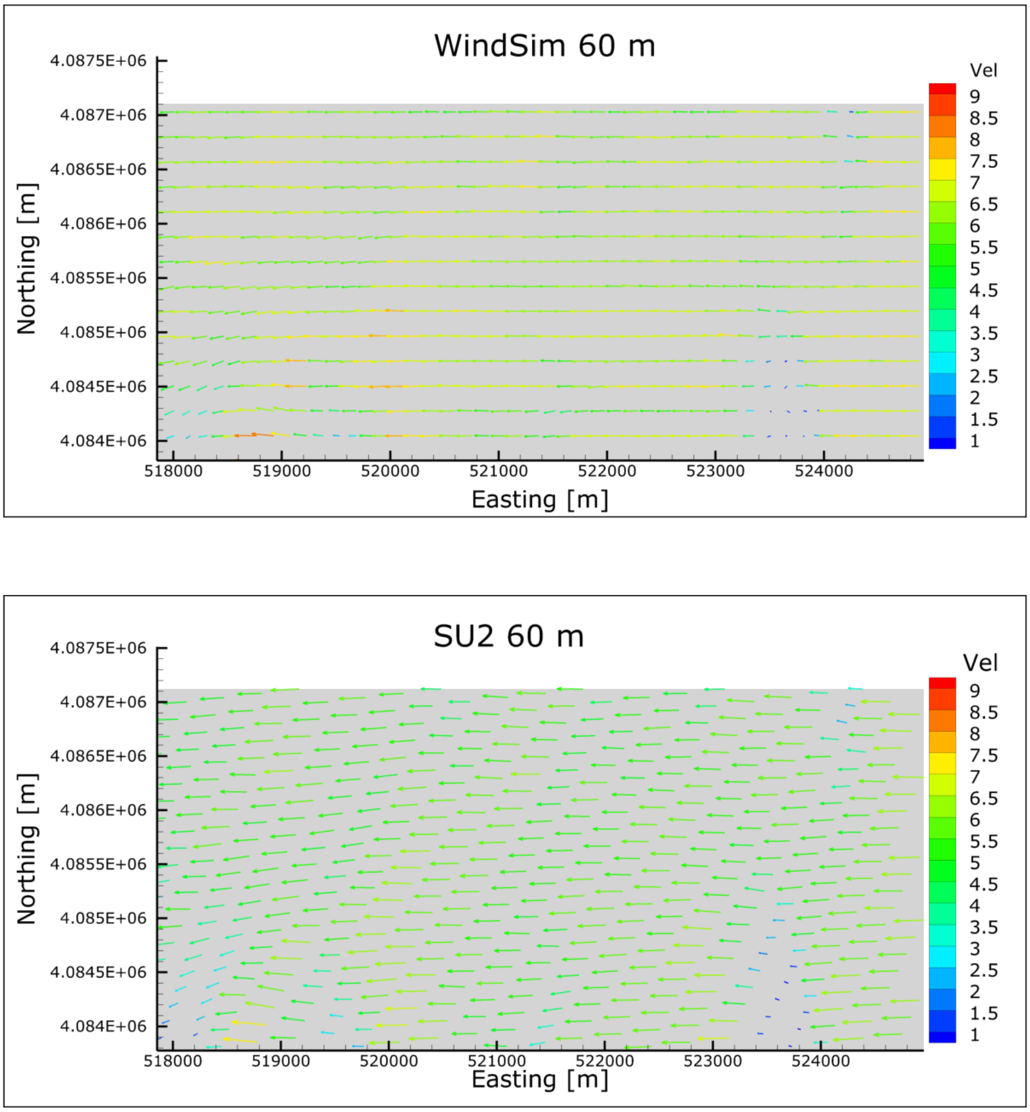

Figure 3.19: 90° sector solution comparison of WindSim and SU^2 at 60m above ground level

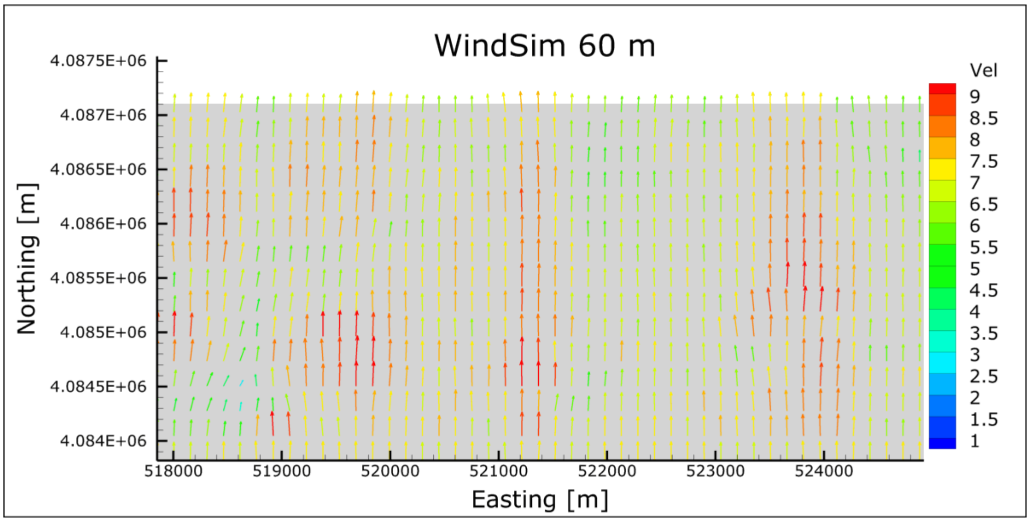

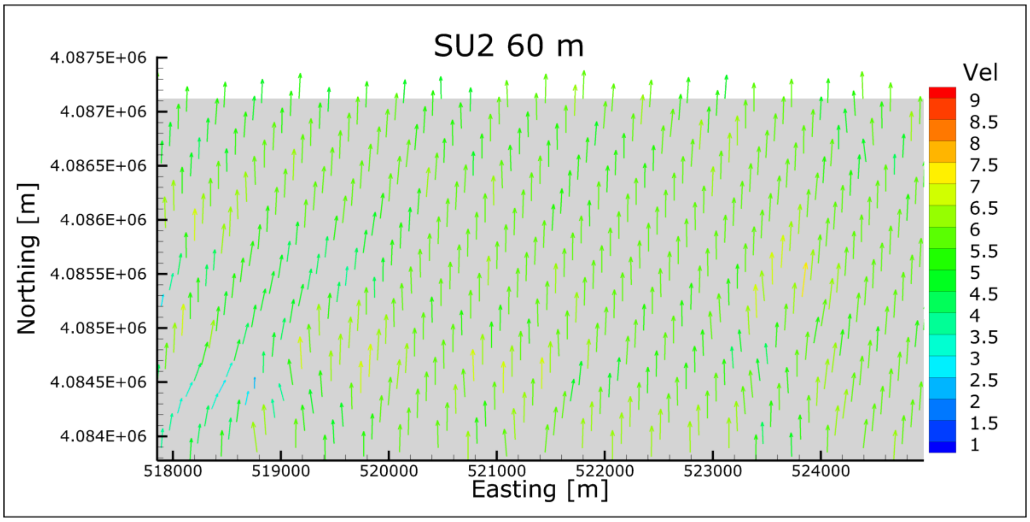

Figure 3.20: 180° sector solution comparison of WindSim and SU^2 at 60m above ground level

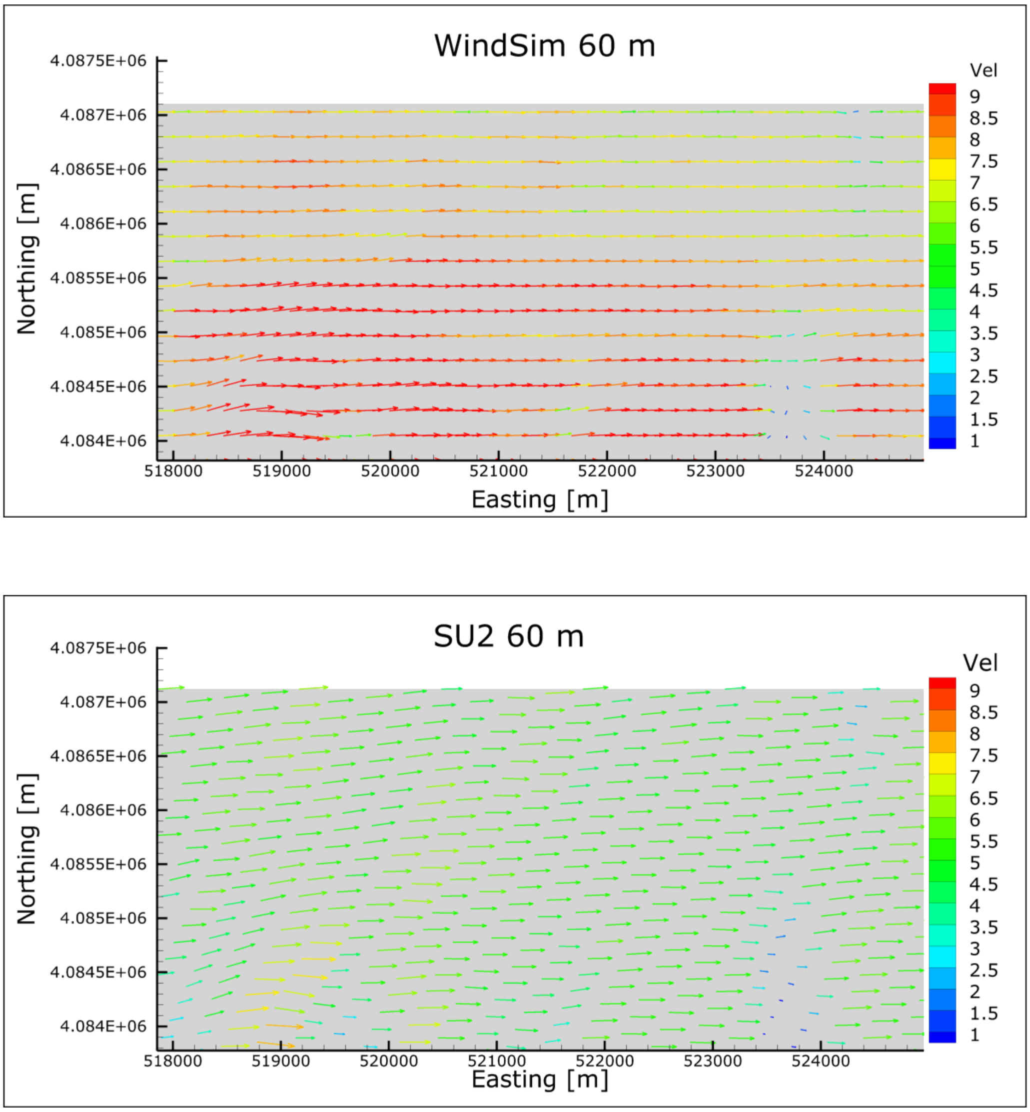

Figure 3.21: 270° sector solution comparison of WindSim and SU^2 at 60m above ground level

method ($x = 521404\ m, y = 4085462\ m$) (Figure 3.23). The steady time series data is created by writing the same solution 100 times. The height of the boundary layer is given as 500 meters to the WindSim software, which is the same BL thickness of the SU^2 simulation, but the results are shown up to 300 meter height because WindSim software outputs are only up to that altitude. Above that height the taking output is not an allowable. The results of arbitrary SU^2 solutions, is reconstructed by POD method applied to the SU^2 sectoral solutions, POD method applied to the WindSim sectoral solutions, and WindSim reconstructions based on the observation point in the arbitrary SU^2 solution Figure 3.24. According to the figure, it is clear that POD application to the SU^2 solutions are in good agreement with the exact solution. The POD application to the WindSim sectoral solution results are match with the SU^2 solutions at observation point. As a results it can be said that, the developed POD method is superior to the WindSim interpolation technique.

Next, wind resource maps obtained from the WindSim and POD method,and they are compared with the SU^2 solutions for 30, 60, 100 and 150 meter heights of same region of the domain (Figure 3.25,Figure 3.26, Figure 3.27 , Figure 3.28). It can be said that POD results are successful for the reconstruction of the flow fields. Near the wall surface flow gradient is high, therefore error near the wall is higher. Once going upward, the error decreases as expected due to flow becomes more stable.

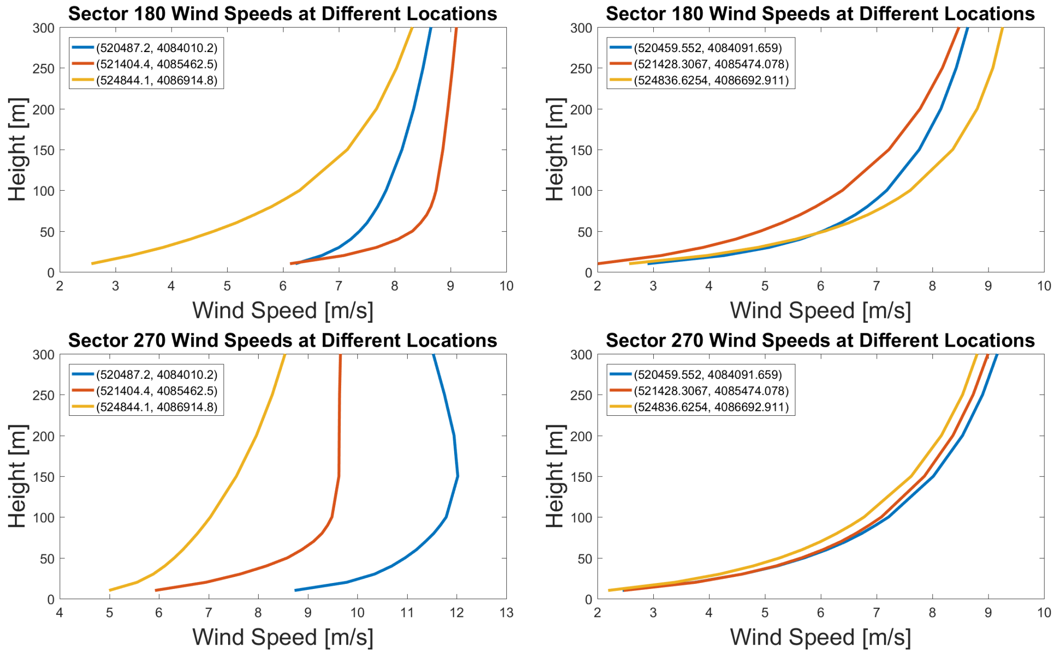

(a) WindSim (b) SU^2

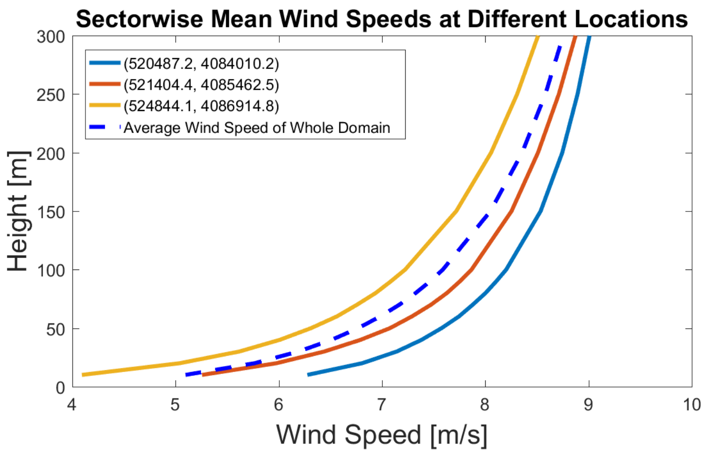

Figure 3.22: Wind speed variation above ground distribution of WindSim at 3 different locations and average wind speed of the all points on the wall surface

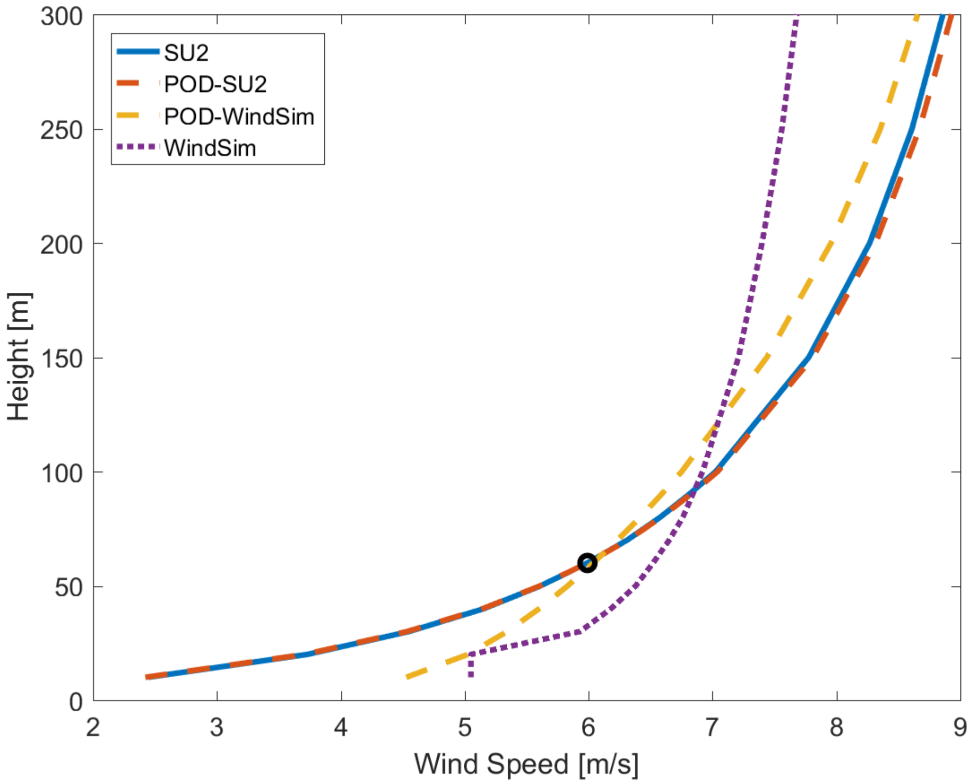

Figure 3.24: SU^2 vs. POD and WindSim wind speed vs. height distribution at the MET-MAST location, $x = 521404\ m, y = 4085462\ m$

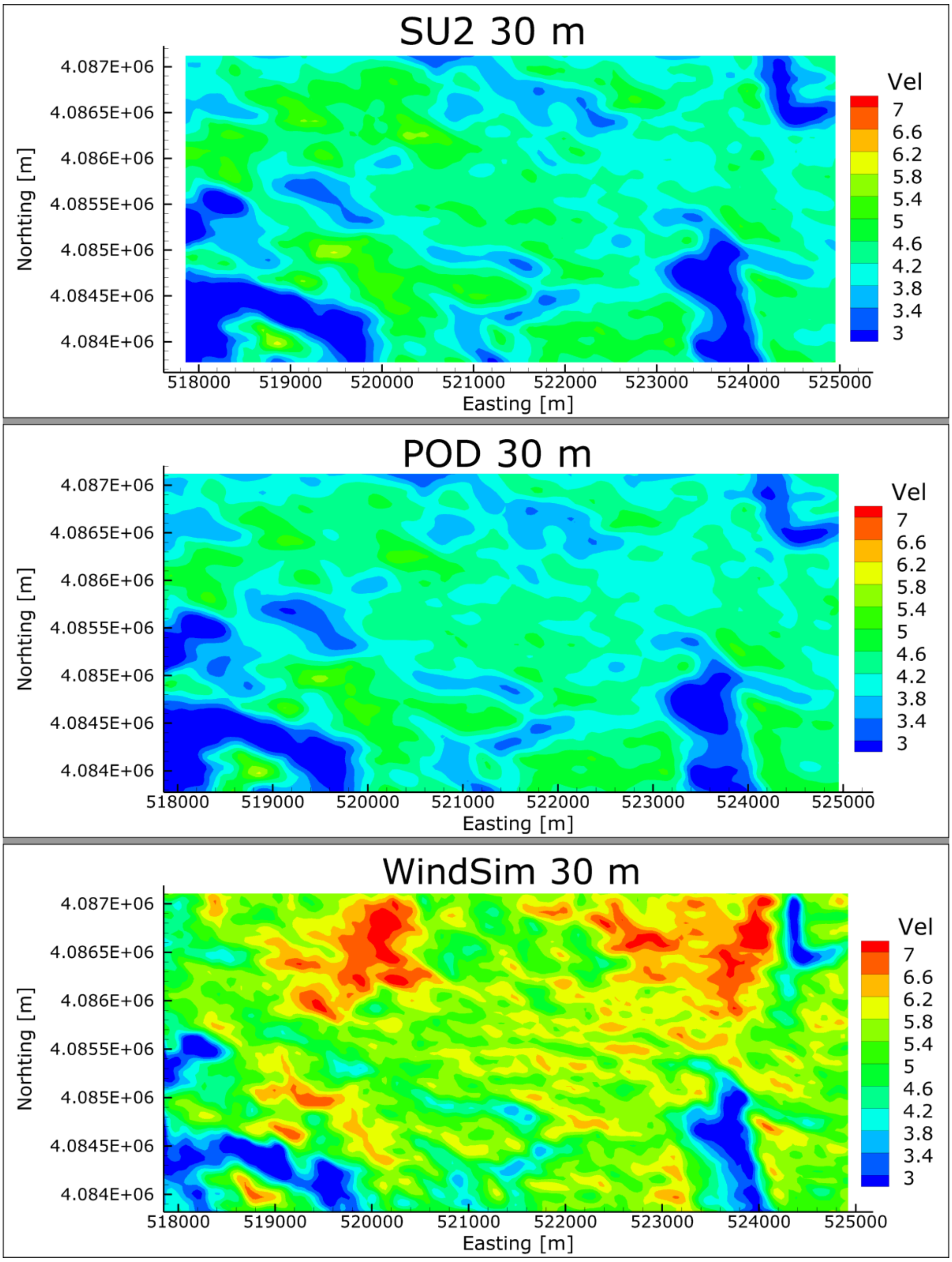

Figure 3.25: SU^2 vs. POD and WindSim wind speed contours [m/s]. 30 meters above from the ground level

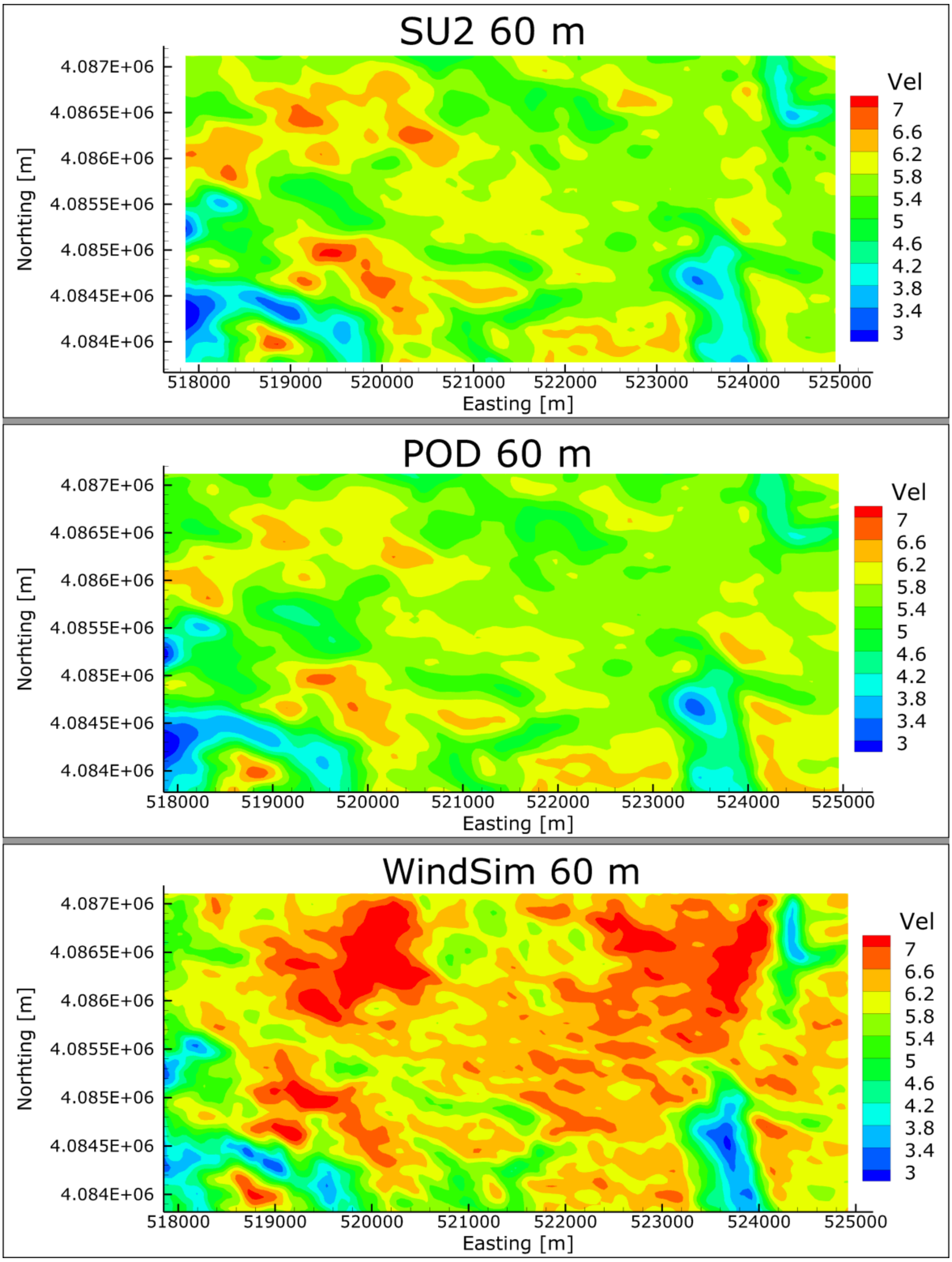

Figure 3.26: SU^2 vs. POD and WindSim wind speed contours [m/s]. 60 meters above from the ground level

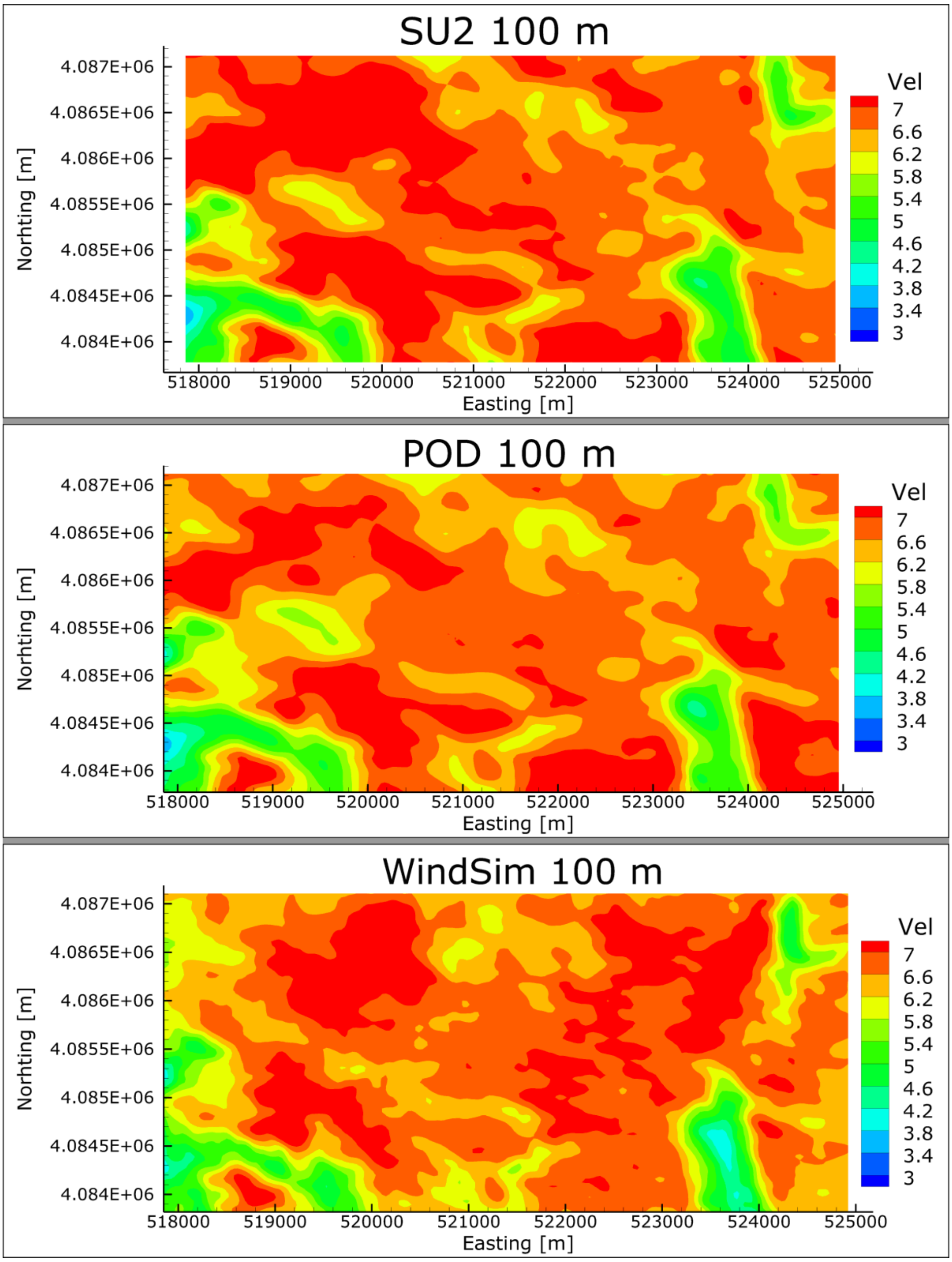

Figure 3.27: SU^2 vs. POD and WindSim wind speed contours [m/s]. 100 meters above from the ground level

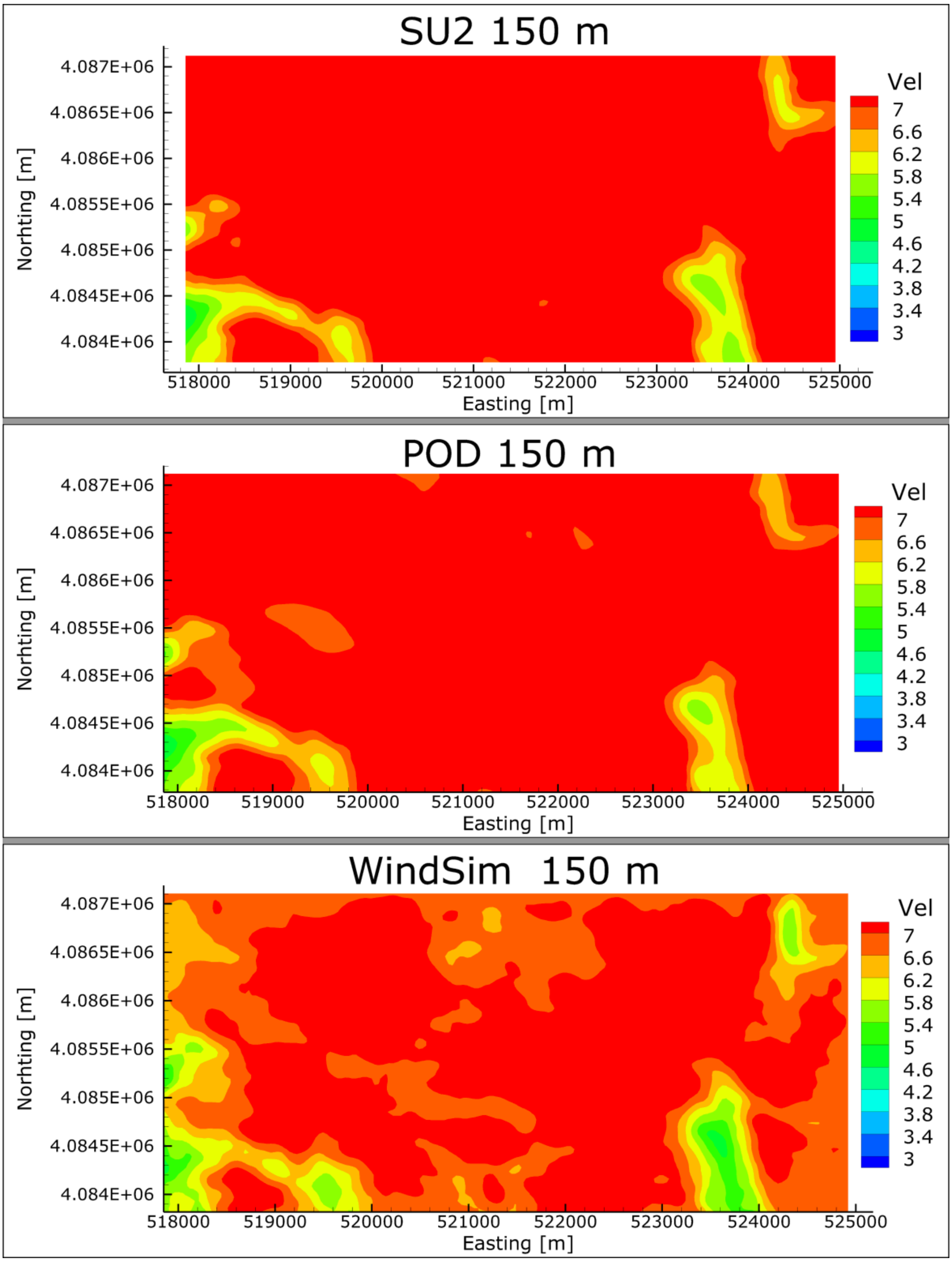

Figure 3.28: SU^2 vs. POD and WindSim wind speed contours [m/s]. 150 meters above from the ground level

CHAPTER 4

CONCLUSIONS

In this study, atmospheric flow fields are successfully reconstructed by means of a POD based methodology and the flow fields computed by an open-source Navier-Stokes solver SU^2. The reconstruction algorithm developed is first validated for 2D flow fields, and then it is implemented in wind farm location for 3D wind fields. Reconstruction of wind fields is based on 12 different sector solutions where the azimuthal wind direction changes in 360°range. Each sector solution corresponds a snapshot in the data set. The sector solutions are obtained with SU^2 flow solver on high resolution terrain fitted grids by imposing the wind speed and direction at the farfield inflow boundaries. It is also shown that turbulent flow solutions with SU^2 on extended solution domains can develop atmosperic boundary layers within the actual flow domain.

It is shown that the POD method successfully captures the dominant characteristics of the sector flow fields, and create a correlation between the solution at grid points within the domain and the dominant flow characteristics. Based on this correlation, the whole flow field can be reconstructed based on the reconstruction variables provided at a small number of point within the solution domain.

The present method developed is also compared with a commercial software WindSim. Although the sectoral flow fields computed by SU^2 and Windsim differ significantly, the reconstructed flowfields are shown to be in agreement.

The results obtained show that the POD based reconstruction method developed in this study can be effectively used for micro-siting of wind turbines in a wind farm and also to make an annual energy production (AEP) estimation of a wind farm. The sectoral wind field solutions and observation data obtained from a met-masts within the wind farm are the only requirements for the reconstruction of the wind field over the wind farm.

The present method can further be developed by improving the turbulence models for atmospheric flows, and simulating the wind turbines with accuator disk/line models.

BIBLIOGRAPHY

[1] Wind atlas analysis and application program. `http://www.wasp.dk/publications`. Accessed: 2016-09-25.

[2] G. Ahmet. *Micro-siting of wind turbines using Navier-Stokes solutions coupled with a numerical weather prediction model*. PhD thesis, Middle East Technical University, 2014.

[3] G. Ahmet, S. Kumru, M. Kaya, and I. H. Tuncer. Meteorolojik hava tahminleri İçin uyumulu dik ayrışım (pod) yöntemiyle veri asimilasyonu. In *Ulusal Havacılık ve Uzay Konferansı (UHUK), Eskişehir, Turkey*, 2010.

[4] B. Blocken, T. Stathopoulos, and J. Carmeliet. Cfd simulation of the atmospheric boundary layer: wall function problems. *Atmospheric environment*, 41(2):238–252, 2007.

[5] T. Bui-Thanh, M. Damodaran, and K. E. Willcox. Aerodynamic data reconstruction and inverse design using proper orthogonal decomposition. *AIAA journal*, 42(8):1505–1516, 2004.

[6] A. Dhunny, M. Lollchund, and S. Rughooputh. Wind energy evaluation for a highly complex terrain using computational fluid dynamics (cfd). *Renewable Energy*, 101:1–9, 2017.

[7] T. D. Economon, F. Palacios, S. R. Copeland, T. W. Lukaczyk, and J. J. Alonso. SU2: An open-source suite for multiphysics simulation and design. *AIAA Journal*, 54(3):828–846, 2016.

[8] T. Glickman. Ams glossary of meteorology. *American Meteorology Society, Boston, USA,*, 2000.

[9] A. Gravdahl and K. Harstveit. Windsim–flow simulations in complex terrain, assessment of wind resources along the norwegian coast. In *5th German Wind Energy Conference*, 2000.

[10] A. Gravdahl, S. Rorgemoen, and M. Thogersen. Power prediction and siting–when the terrain gets rough. In *The World Wind Energy Conference and Exhibition*, pages 1–4. Citeseer, 2002.

[11] P. Holmes, J. L. Lumley, and G. Berkooz. *Turbulence, coherent structures, dynamical systems and symmetry*. Cambridge university press, 1998.

[12] J. Y. Kuo, D. A. Romero, J. C. Beck, and C. H. Amon. Wind farm layout optimization on complex terrains–integrating a cfd wake model with mixed-integer programming. *Applied Energy*, 178:404–414, 2016.

[13] L. Landberg, L. Myllerup, O. Rathmann, E. L. Petersen, B. H. Jørgensen, J. Badger, and N. G. Mortensen. Wind resource estimation an overview. *Wind Energy*, 6(3):261–271, 2003.

[14] E. Leblebici, G. Ahmet, and I. H. Tuncer. Atmospheric turbulent flow solutions coupled with a mesoscale weather prediction model. In *Torque Conference, Oldenburg, Germany*, 2012.

[15] Y. Liang, H. Lee, S. Lim, W. Lin, K. Lee, and C. Wu. Proper orthogonal decomposition and its applications part i: Theory. *Journal of Sound and vibration*, 252(3):527–544, 2002.

[16] L. Lu and K. Sun. Wind power evaluation and utilization over a reference highrise building in urban area. *Energy and Buildings*, 68:339–350, 2014.

[17] C. Meissner. Windsim 5, getting started, 2010.

[18] A. Mochida, Y. Tominaga, and R. Yoshie. Aij guideline for practical applications of cfd to wind environment around buildings. In *4th International Symposium on Computational Wind Engineering (CWE2006)*, 2006.

[19] N. G. Mortensen, D. N. Heathfield, L. Myllerup, L. Landberg, and O. Rathmann. Wind atlas analysis and application program: Wasp 9 help facility, 2007.

[20] H. Mu, W. Wei, A. Untaroiu, and Q. Yan. Study on reconstruction and prediction methods of pressure field on blade surfaces for oil-filling process in a hydrodynamic retarder. *International Journal of Numerical Methods for Heat & Fluid Flow*, 26(6):1843–1870, 2016.

[21] Y. Ni and M. Li. Wind pressure data reconstruction using neural network techniques: A comparison between bpnn and grnn. *Measurement*, 88:468–476, 2016.

[22] F. Palacios, M. R. Colonno, A. C. Aranake, A. Campos, S. R. Copeland, T. D. Economon, A. K. Lonkar, T. W. Lukaczyk, T. W. Taylor, and J. J. Alonso. Stanford university unstructured (su2): An open-source integrated computational environment for multi-physics simulation and design. *AIAA Paper*, 287:2013, 2013.

[23] L. Perković, P. Silva, M. Ban, N. Kranjčević, and N. Duić. Harvesting high altitude wind energy for power production: The concept based on magnus effect. *Applied energy*, 101:151–160, 2013.

[24] W. H. Schilders, H. A. Van der Vorst, and J. Rommes. *Model order reduction: theory, research aspects and applications*, volume 13. Springer, 2008.

[25] L. Sirovich and M. Kirby. Low-dimensional procedure for the characterization of human faces. *Josa a*, 4(3):519–524, 1987.

[26] M. Song, K. Chen, X. Zhang, and J. Wang. The lazy greedy algorithm for power optimization of wind turbine positioning on complex terrain. *Energy*, 80:567–574, 2015.

[27] A. WindSIM. Windsim 4.8. 1 getting started, 2008.